Dimethylsulfoxide as a Ligand for Rh^I and Ir^I Complexes—Isolation, Structure, and Reactivity Towards X–H Bonds (X = H, OH, OCH_3)**

Reto Dorta,[a] Haim Rozenberg,[b] Linda J. W. Shimon,[b] and David Milstein*[a]

Abstract: Novel neutral and cationic Rh^I and Ir^I complexes that contain only DMSO molecules as dative ligands with S-, O-, and bridging S,O-binding modes were isolated and characterized. The neutral derivatives $[RhCl(DMSO)_3]$ (**1**) and $[IrCl(DMSO)_3]$ (**2**) were synthesized from the dimeric precursors $[M_2Cl_2(coe)_4]$ (M = Rh, Ir; COE = cyclooctene). The dimeric Ir^I compound $[Ir_2Cl_2(DMSO)_4]$ (**3**) was obtained from **2**. The first example of a square-planar complex with a bidentate S,O-bridging DMSO ligand, [(coe)(DMSO)Rh-(μ-Cl)(μ-DMSO)RhCl(DMSO)] (**4**), was obtained by treating $[Rh_2Cl_2(coe)_4]$ with three equivalents of DMSO. The mixed DMSO–olefin complex [IrCl-(cod)(DMSO)] (**5**, COD = cyclooctadiene) was generated from $[Ir_2Cl_2-(cod)_2]$. Substitution reactions of these neutral systems afforded the complexes $[RhCl(py)(DMSO)_2]$ (**6**), $[IrCl(py)-(DMSO)_2]$ (**7**), $[IrCl(iPr_3P)(DMSO)_2]$ (**8**), [RhCl(dmbpy)(DMSO)] (**9**, dmbpy = 4,4′-dimethyl-2,2′-bipyridine), and [IrCl(dmbpy)(DMSO)] (**10**). The cationic O-bound complex $[Rh(cod)(DMSO)_2]BF_4$ (**11**) was synthesized from $[Rh(cod)_2]BF_4$. Treatment of the cationic complexes $[M(coe)_2(O{=}C-Me_2)_2]PF_6$ (M = Rh, Ir) with DMSO gave the mixed S- and O-bound DMSO complexes $[M(DMSO)_2(DMSO)_2]PF_6$ (Rh = **12**; Ir = in situ characterization). Substitution of the O-bound DMSO ligands with dmbpy or pyridine resulted in the isolation of $[Rh(dmbpy)(DMSO)_2]PF_6$ (**13**) and $[Ir(py)_2(DMSO)_2]PF_6$ (**14**). Oxidative addition of hydrogen to $[IrCl(DMSO)_3]$ (**2**) gave the kinetic product *fac*-$[Ir(H)_2Cl(DMSO)_3]$ (**15**) which was then easily converted to the more thermodynamically stable product *mer*-$[Ir(H)_2Cl(DMSO)_3]$ (**16**). Oxidative addition of water to both neutral and cationic Ir^I DMSO complexes gave the corresponding hydrido–hydroxo addition products *syn*-$[(DMSO)_2HIr(\mu\text{-}OH)_2-(\mu\text{-}Cl)IrH(DMSO)_2][IrCl_2(DMSO)_2]$ (**17**) and *anti*-$[(DMSO)_2(DMSO)HIr(\mu\text{-}OH)_2-IrH(DMSO)_2(DMSO)][PF_6]_2$ (**18**). The cationic $[Ir(DMSO)_2(DMSO)_2]PF_6$ complex (formed in situ from $[Ir(coe)_2(O{=}C-Me_2)_2]PF_6$) also reacts with methanol to give the hydrido–alkoxo complex *syn*-$[(DMSO)_2HIr(\mu\text{-}OCH_3)_3IrH(DMSO)_2]-PF_6$ (**19**). Complexes **1**, **2**, **4**, **5**, **11**, **12**, **14**, **17**, **18**, and **19** were characterized by crystallography.

Keywords: iridium · O ligands · oxidative addition · rhodium · S ligands

Introduction

Soluble, low-valent rhodium and iridium systems have attracted much attention in the past decades showing a wide range of reactivity and being applied very successfully as homogeneous catalysts.[1] Such compounds are normally stabilized with phosphine ligands, but as these ligands are highly air sensitive, toxic, and expensive, there is a growing interest in finding alternate ligands that show similar characteristics. Among them, sulfoxides seem to be particularly interesting. We were, therefore, surprised to see that although their coordination chemistry has been widely studied,[2] well-characterized Rh^I– and Ir^I–DMSO complexes that do not contain other dative ligands are unknown.[3] This is all the more perplexing, since some high-valent Rh^{III}– and Ir^{III}–DMSO complexes have been applied successfully as catalysts for various transformations.[4] For the developement of new catalysts based on low-valent transition-metal complexes, detailed investigation of substitution chemistry and oxidative addition reactions is crucial. Within this latter category, oxidative addition of OH groups by transition-metal complexes has received much attention in recent years by virtue of its relevance to a number of catalytic processes, and its potential importance in the design of new catalysts based on water.[5] Examples of hydrido–hydroxo and hydrido–alkoxo complexes generated by OH oxidative addition are rare, and

[a] Prof. D. Milstein, R. Dorta
Department of Organic Chemistry
The Weizmann Institute of Science
Rehovot 76100 (Israel)
Fax: (+972) 8934-4142
E-mail: david.milstein@weizmann.ac.il

[b] Dr. H. Rozenberg, Dr. L. J. W. Shimon
Unit of Chemical Research Support
The Weizmann Institute of Science
Rehovot 76100 (Israel)

[**] Throughout this paper the coordination of the DMSO ligand is indicated in the compound formulae by the S of DMSO being italicized for sulfur coordination and the O for oxygen coordination.

 DOI: 10.1002/chem.200305144

this reactivity is usually achieved by using late-transition-metal complexes that bear phosphine ligands.[6]

Herein, we describe the synthesis of neutral and cationic Rh^I and Ir^I complexes that contain DMSO as the only (or main) ligand. Most of these new complexes were unambiguously characterized by X-ray crystallography, and showed both S- and O-bonding modes of the DMSO ligand. In addition, we have characterized a binuclear rhodium complex that contains a rare S,O-bridging DMSO ligand. We present studies on the substitution behavior of these complexes, and, in the case of the Ir^I DMSO systems, the reactivity displayed towards X–H bonds. Not only was oxidative addition of hydrogen observed, but the iridium complexes showed surprising reactivity towards the polar O–H bonds of water and methanol. These substrates underwent oxidative addition at room temperature to afford addition products that were characterized by X-ray diffraction. This is the first time that such reactivity has been observed for phosphine-free late transition metals. Some of the results described herein have been previously published in a communication.[7]

Results and Discussion

Synthesis, structure, and substitution chemistry of neutral M^I DMSO complexes (M = Rh, Ir): Reaction of a toluene slurry of $[M_2Cl_2(coe)_4]$ (M = Rh, Ir; coe = cyclooctene) with excess DMSO and subsequent workup led to the formation of the neutral complexes $[RhCl(DMSO)_3]$ (**1**) and $[IrCl(DMSO)_3]$ (**2**) in high yield (Scheme 1). The ^1H NMR spectrum of the yellow complex **1** in CD_2Cl_2 consists of a single broad resonance at 3.19 ppm,[8] indicating that dissociation of DMSO occurs rapidly on the NMR timescale. In fact, low-temperature ^1H NMR analysis gave rise to the appearance of two separate broad resonances at 243 K, but the signals for the coordinated DMSO molecules were not sharp even at 183 K.

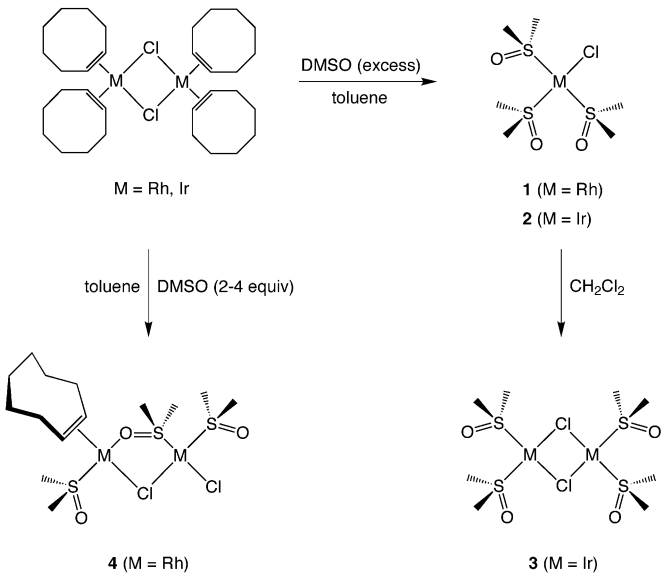

Scheme 1.

Interestingly, in the case of the lemon-yellow iridium complex **2**, dissolution in CH_2Cl_2 was accompanied by an immediate color change to orange and by loss of one equivalent of DMSO. Addition of diethyl ether led to the precipitation of the dimer $[Ir_2Cl_2(DMSO)_4]$ (**3**) as an orange, microcrystalline solid in 95 % yield (Scheme 1). The ^1H NMR spectrum of **3** in CD_2Cl_2 consists of two broad singlet resonances at 3.47 and 3.64 ppm; this indicates that the DMSO molecules are part of a dynamic process. In fact, gradual lowering of the temperature showed what appeared to be two independent dynamic processes, taking place between 273 – 253 K and 233 – 203 K. When the temperature is further lowered to 193 K, eight sharp signals can be seen between 3.29 and 3.79 ppm. As no other signals apart from the methyl resonances of the DMSO ligands are present, we cannot determine with certainty whether these signals arise from different conformers of **3** or if they are the result of all the eight methyl resonances being differentiable at 193 K. Nevertheless, the eight signals are of equal intensity; this implies that it is less likely that they are due to conformers (which would probably differ in stability). Similar behavior to that observed for complex **3** was recently observed in the case of the Ir^{III} complex $[Cp^*Ir(DMSO)_3][PF_6]_2$.[9] In contrast to the Ir^{III} complex, rapid exchange between bound and free DMSO was not observed for **3**, even when the temperature of a CD_2Cl_2 solution of **3** in the presence of free DMSO was lowered. The structures of complexes **1** – **3** are supported by elemental analyses, and in the case of compounds **1** and **2**, single crystals suitable for X-ray diffraction studies were grown directly from more dilute reaction mixtures. The ORTEP views, along with selected bond lengths and angles are shown in Figure 1. Both complexes are monomeric and show the expected square-planar geometry around the metal center, with one chloride ligand and all three DMSO molecules bound through the sulfur atom. In both complexes, the M–S bond lengths for the DMSO molecules *cis* to the chloride (2.2722(11) and 2.2874(11) Å for **1**, 2.2643(10) and 2.2763(10) Å for **2**) are significantly longer than for the DM*S*O molecules *trans* to Cl (2.2095(11) Å for **1**, 2.1957(9) Å for **2**); this indicates that S-bound DMSO has a higher *trans* influence than the chloride. The relatively long metal – sulfur distances for the DM*S*O ligands *trans* to each other might also explain the labile nature of these ligands in solution.[10] As observed for **1**, Wilkinson's catalyst $[RhCl(PPh_3)_3]$ undergoes phosphine dissociation in solution, and has a chemically unique rhodium – phosphorus bond that is substantially shorter than the other two (2.214(4) Å as compared to 2.322(4) and 2.334(3) Å).[11, 12]

Interestingly, treatment of a dilute solution of $[Rh_2Cl_2(coe)_4]$ in toluene with 2 – 4 equivalents of DMSO led to the formation of crystals, although in lower yield than that for complex **1** (Scheme 1). X-ray crystallography revealed that the crystals consisted of the doubly-bridged dimer [(coe)(DM*S*O)Rh(μ-Cl)(μ-DM*S*O)RhCl(DM*S*O)] (**4**) in Figure 2. Structurally characterized sulfoxides that bridge two transition metals are extremely rare and have only been reported for two octahedral diruthenium complexes,[13, 14] and two octahedral rhodium(II) complexes.[15] In complex **4**, both metal atoms achieve a nearly square-planar environment. The Rh–S bond length for the S-bound DMSO molecule *trans* to

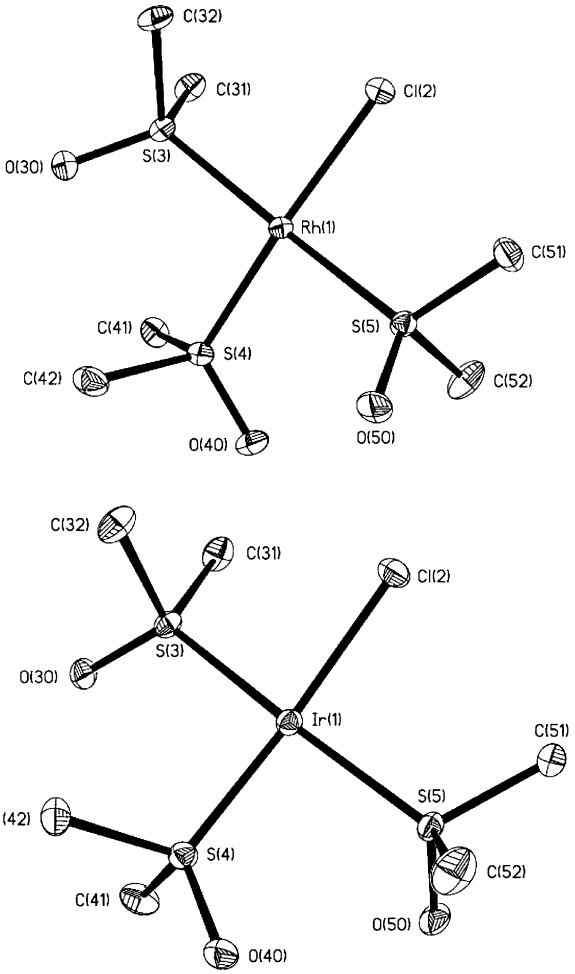

Figure 1. ORTEP plots (50% probability) of $RhCl(DMSO)_3$ (**1**, above) and $[IrCl(DMSO)_3]$ (**2**, below). Hydrogen atoms have been omitted for clarity. Selected bond lengths [Å] and angles [°] for **1**: Rh(1)–S(4) 2.2095(11), Rh(1)–S(3) 2.2722(11), Rh(1)–S(5) 2.2874(11), Rh(1)–Cl(2) 2.3555(11), S(3)–O(30) 1.485(3), S(4)–O(40) 1.481(3), S(5)–O(50) 1.489(3), S(4)-Rh(1)-S(3) 93.72(4), S(4)-Rh(1)-S(5) 90.22(4), S(3)-Rh(1)-S(5) 169.86(4), S(4)-Rh(1)-Cl(2) 168.63(4), S(3)-Rh(1)-Cl(2) 86.84(4), S(5)-Rh(1)-Cl(2) 91.14(4); for **2**: Ir(1)–S(4) 2.1957(9), Ir(1)–S(3) 2.2643(10), Ir(1)–S(5) 2.2763(10), Ir(1)–Cl(2) 2.3566(10), S(3)–O(30) 1.482(3), S(4)–O(40) 1.486(3), S(5)–O(50) 1.483(3), S(4)-Ir(1)-S(3) 93.61(4), S(4)-Ir(1)-S(5) 90.04(4), S(3)-Ir(1)-S(5) 170.34(3), S(4)-Ir(1)-Cl(2) 169.95(3), S(3)-Ir(1)-Cl(2) 86.79(4), S(5)-Ir(1)-Cl(2) 91.18(4).

the bridging chloride (2.1965(10) Å) is similar to that found for the DMSO ligand *trans* to chloride in complex **1**. Interestingly, the Rh(2)–S(7) distance for the bridging DMSO, which is also *trans* to a chloride, is significantly shorter (2.1584(9) Å). The S=O bond length for the bridging DMSO (S(7)–O(70) 1.521(2) Å) is longer than in corresponding S-bound complexes, and approaches the values found in the O-bound DMSO molecules of $[Rh(cod)(DMSO)_2]BF_4$ (**11**) and $[Rh(DMSO)_4]PF_6$ (**12**) (see below), or the two known O-bound Rh^{III}–DMSO complexes.[16, 17] Indeed, in complex **1**, we generally find longer metal–ligand bonds; this is consistent with the relative stability of the unusual complex **4**.

To get a better idea about the ligating ability of DMSO with respect to Rh^I and Ir^I, we investigated whether complexes **1**, **2**, and **3** could also be obtained from $[M_2Cl_2(cod)_2]$ (M = Rh, Ir; COD = cyclooctadiene) rather than just from the non-chelating olefin complexes $[M_2Cl_2(coe)_4]$. Therefore, we treated an orange solution of $[Rh_2Cl_2(cod)_2]$ in toluene with excess DMSO in a manner analogous to the preparation of **1** from $[Rh_2Cl_2(coe)_4]$. The solution was stirred at room temperature and subsequent workup resulted in the recovery of the starting material according to the ^1H NMR spectrum. However, the ^1H NMR spectrum of the reaction solution (in $[D_8]$toluene) revealed broad signals for the vinylic protons of COD, indicating what appears to be fast and reversible binding of DMSO to the starting complex. In contrast, when an orange solution of $[Ir_2Cl_2(cod)_2]$ in toluene was treated with excess DMSO, the solution turned yellow. After being stirred at room temperature for five hours and subsequent workup, a dark yellow powder was isolated in 86% yield. The ^1H NMR spectrum in $[D_6]$benzene showed that the cyclooctadiene ligand was still coordinated to the metal center, and the signal at 2.56 ppm indicated the presence of only one S-bound DMSO ligand (COD/DMSO = 1:1). Thus, the resulting complex has the formula [IrCl(cod)(DMSO)] (**5**), which was supported by elemental analysis (Scheme 2). This

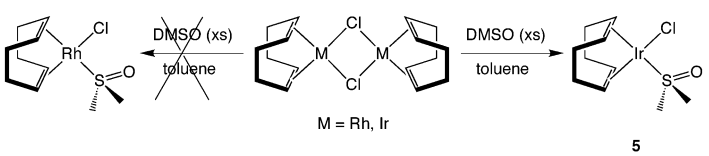

Scheme 2.

means that for both Rh and Ir, the DMSO ligand is incapable of displacing a chelating olefin ligand such as cyclooctadiene, and that only in the case of iridium, the chloride bridge is irreversibly split and leads to the formation of the monomeric

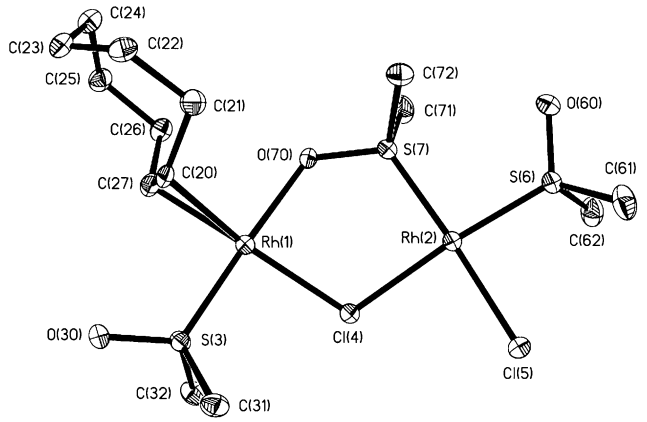

Figure 2. ORTEP view of a molecule of **4**. Thermal ellipsoids are drawn at the 50% probability level. Hydrogen atoms have been omitted for clarity. Selected bond lengths [Å] and angles [°]: Rh(1)–O(70) 2.112(2), Rh(1)–C(20) 2.133(3), Rh(1)–C(27) 2.154(3), Rh(1)–S(3) 2.1610(10), Rh(1)–Cl(4) 2.3812(10), Rh(2)–S(7) 2.1584(9), Rh(2)–S(6) 2.1965(10), Rh(2)–Cl(5) 2.3503(9), Rh(2)–Cl(4) 2.3785(10), S(3)–O(30) 1.479(2), S(6)–O(60) 1.480(2), S(7)–O(70) 1.521(2), O(70)-Rh(1)-C(20) 92.48(10), O(70)-Rh(1)-C(27) 91.28(10), C(20)-Rh(1)-C(27) 38.04(11), O(70)-Rh(1)-S(3) 174.08(6), C(20)-Rh(1)-S(3) 91.99(9), C(27)-Rh(1)-S(3) 89.85(9), O(70)-Rh(1)-Cl(4) 86.06(6), C(20)-Rh(1)-Cl(4) 157.34(8), C(27)-Rh(1)-Cl(4) 164.39(8), S(3)-Rh(1)-Cl(4) 91.30(3), S(7)-Rh(2)-S(6) 94.24(4), S(7)-Rh(2)-Cl(5) 176.96(3), S(6)-Rh(2)-Cl(5) 88.81(4), S(7)-Rh(2)-Cl(4) 90.14(4), S(6)-Rh(2)-Cl(4) 174.01(3), Cl(5)-Rh(2)-Cl(4) 86.83(3).

complex **5**. This reactivity parallels that observed for the phosphine ligands PPh_3 and PCy_3, whereby complexes of the type [IrCl(cod)L] (L = PPh_3, PCy_3) are obtained even in the presence of excess phosphine.[18, 19] The structure of **5** was confirmed by an X-ray diffraction study of suitable orange crystals, which were grown from a saturated diethyl ether solution. The ORTEP diagram of [IrCl(cod)(DM*SO*)] (**5**), along with selected bond lengths and angles is shown in Figure 3. The Ir–S bond length of 2.268(2) Å is similar to

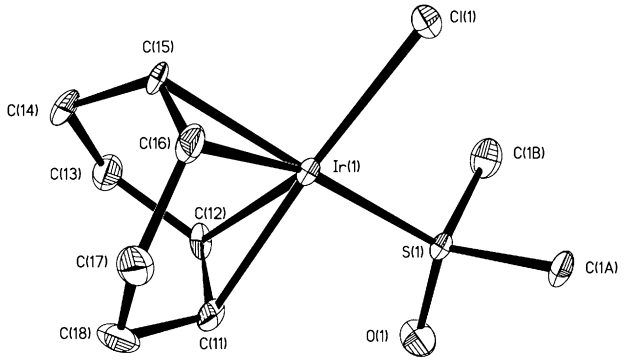

Figure 3. ORTEP view of a molecule of **5** (one of two independant molecules). Thermal ellipsoids are drawn at the 50% probability level. Hydrogen atoms have been omitted for clarity. Selected bond lengths [Å] and angles [°]: Ir(1)–C(12) 2.091(8), Ir(1)–C(11) 2.149(8), Ir(1)–C(16) 2.180(8), Ir(1)–C(15) 2.196(7), Ir(1)–S(1) 2.268(2), Ir(1)–Cl(1) 2.350(2), S(1)–O(1) 1.467(6), C(12)-Ir(1)-C(11) 38.0(3), C(12)-Ir(1)-C(16) 97.6(3), C(11)-Ir(1)-C(16) 81.6(3), C(12)-Ir(1)-C(15) 82.0(3), C(11)-Ir(1)-C(15) 89.3(3), C(16)-Ir(1)-C(15) 36.8(3), C(12)-Ir(1)-S(1) 91.7(2), C(11)-Ir(1)-S(1) 91.7(2), C(16)-Ir(1)-S(1) 154.6(2), C(15)-Ir(1)-S(1) 168.5(2), C(12)-Ir(1)-Cl(1) 154.0(3), C(11)-Ir(1)-Cl(1) 167.7(2), C(16)-Ir(1)-Cl(1) 91.1(2), C(15)-Ir(1)-Cl(1) 90.7(2).

those found for two of the three Ir–S bonds in the DMSO-stabilized complex [IrCl(DM*SO*)$_3$] (**2**), and confirms the observation that the *trans* influence of S-bound DMSO is significantly higher compared to chloride. This is also apparent from the Ir–olefin bond lengths *trans* to these ligands, in which the average Ir–olefin distance is 2.120 Å for the olefin opposite the chloride, and 2.188 Å for the olefin opposite the DMSO ligand. The ^{1}H NMR spectrum also reflects these findings as the olefin protons appear at 5.00 ppm (*trans* to DMSO) and 4.00 ppm (*trans* to Cl). The differences in the *trans* influence that DMSO and olefins display are much more subtle, but the bond lengths in complexes **2** and **5** indicate that S-bound DMSO has a slightly higher *trans* influence relative to the double bonds of cyclooctadiene. In line with this assuption is the fact that DMSO did not dissociate when complex **5** was dissolved in dichloromethane, in contrast to complex **2**, which afforded dimer **3**.

Substitution of the DMSO ligands in **1**, **2**, and **3** was subsequently investigated. An orange [D$_6$]benzene suspension of **1** was treated with excess pyridine to give a yellow solution of [RhCl(py)(DM*SO*)$_2$] (**6**) (py = pyridine) and one equivalent of free DMSO (Scheme 3). The iridium complex **2** behaved in an identical manner; treatment of a solution of **2** in acetone with excess pyridine and subsequent workup led to the isolation of the corresponding complex [IrCl(py)(DM*SO*)$_2$] (**7**). These complexes were characterized by NMR

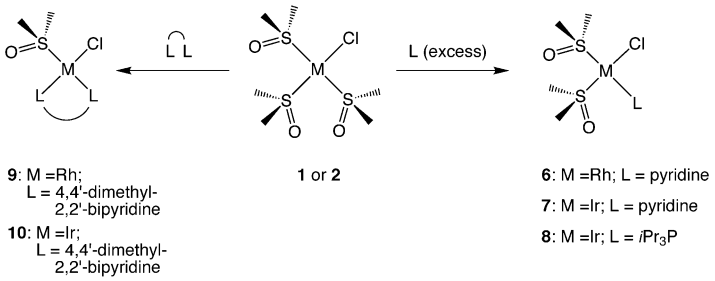

Scheme 3.

spectroscopy and elemental analysis. The ^{1}H NMR spectra show two sharp signals for the methyl protons of the two non-equivalent DMSO ligands of the square-planar complexes at 3.01 and 3.03 ppm for **6** (in [D$_6$]benzene; 3.21 and 3.23 ppm in [D$_6$]acetone), and at 3.40 and 3.48 ppm for **7** (CD_2Cl_2); this confirms the S-bound mode of DMSO in both cases. The NMR spectra are completed by peaks in the aromatic region that correspond to the pyridine ligand.

Treatment of complexes **2** and **3** with triisopropylphosphine was attempted to see how many DMSO molecules could be substituted by this ligand. Interestingly, reaction of **2** (or **3**) with either an equimolar amount or an excess of triisopropylphosphine led to the isolation of the same complex, [IrCl(*i*Pr$_3$P)(DM*SO*)$_2$] (**8**), the structure of which was confirmed by NMR spectroscopy and elemental analysis (Scheme 3). The ^{1}H NMR spectrum in [D$_6$]benzene contains two signals for the S-bound DMSO molecules at 2.91 and 3.40 ppm, and two signals for the phosphine ligand (quartet at 1.34 ppm and multiplet at 3.09 ppm). The ^{31}P NMR spectrum shows a single peak at 34.24 ppm. We observe that rather unexpectedly, only one of the DMSO ligands can be displaced even in presence of "good" ligands (for Ir^I), such as *i*Pr$_3$P. In contrast, all the olefin ligands of [Ir$_2$Cl$_2$(coe)$_4$], which is formally the olefin analogue of **3**, are substitued with phosphine ligands; this is why monomeric, neutral Ir–monophosphine complexes (without bi- or tri-dentate ligands) are exceedingly rare. The only two such complexes that we are aware of are the mixed phosphine/stibine complexes [IrCl(C$_2$H$_4$)(*i*Pr$_3$Sb)(*i*Pr$_3$P)] and [IrCl(=CR$_2$)(*i*Pr$_3$Sb)(*i*Pr$_3$P)].[20] This reactivity once again indicates that the DMSO ligand (S-bound) is more strongly bound to M^I than a simple olefin ligand such as COE.

Not surprisingly, it is possible to substitute more than one DMSO ligand when chelating ligands are employed. Reaction of **1** with one equivalent of the chelating ligand dmbpy (dmbpy = 4,4′-dimethyl-2,2′-bipyridine) gave complex [RhCl(dmbpy)(DM*SO*)] (**9**) with concomitant loss of two equivalents of DMSO (Scheme 3).[21] The corresponding iridium complex, [IrCl(dmbpy)(DM*SO*)] (**10**), was obtained in a similar manner from complex **2**.[22]

Synthesis, structure, and substitution reactivity of cationic M^I DMSO systems (M = Rh, Ir): The starting point of our investigations stemmed from two reports on the synthesis of the cationic Rh^I complexes [Rh(diene)(DMSO)(L)]X (L = phosphine, DMSO, X = BF_4^-, PF_6^-).[23, 24] Based on IR spectroscopic data and their lability in solution, these com-

plexes were believed to have O-bound DMSO ligands. To ascertain the exact structure of these compounds, we synthesized complex $[Rh(cod)(DMSO)_2]BF_4$ (**11**) and characterized it by X-ray crystallogrphy. Crystals suitable for X-ray analysis were grown from a concentrated dichloromethane solution. Complex **11** crystallizes in the orthorhombic space group $Pca2_1$ as two crystallographically distinct molecules, which display some differences in their corresponding bond lengths and angles.[25] An ORTEP drawing of one molecule along with selected bond lengths and angles is shown in Figure 4. The

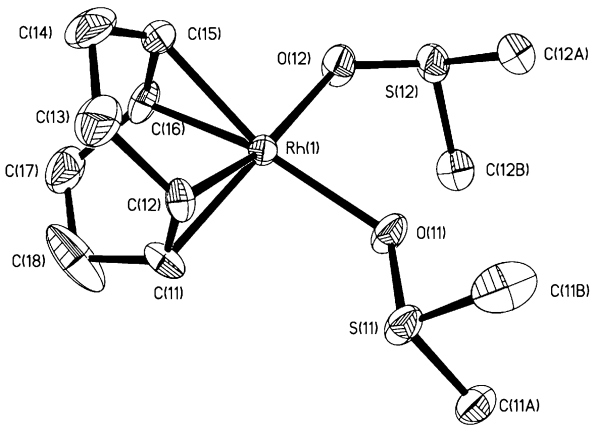

Figure 4. ORTEP plot of a molecule of **11** (one of two independant molecules). Thermal ellipsoids are drawn at the 50 % probability level. The BF_4^- counterion and hydrogen atoms have been omitted for clarity. Selected bond lengths [Å] and angles [°]: Rh(1)–C(11) 2.092(5), Rh(1)–C(12) 2.101(4), Rh(1)–C(16) 2.106(5), Rh(1)–C(15) 2.117(5), Rh(1)–O(11) 2.107(3), Rh(1)–O(12) 2.128(3), S(11)–O(11) 1.536(3), S(12)–O(12) 1.528(4), C(11)-Rh(1)-C(12) 38.80(19), C(11)-Rh(1)-C(16) 81.9(2), C(12)-Rh(1)-C(16) 94.0(2), C(11)-Rh(1)-O(11) 94.40(18), C(12)-Rh(1)-O(11) 95.34(16), C(16)-Rh(1)-O(11) 159.81(19), C(11)-Rh(1)-C(15) 94.7(2), C(12)-Rh(1)-C(15) 81.4(2), C(16)-Rh(1)-C(15) 39.0(2), O(11)-Rh(1)-C(15) 160.81(19), C(11)-Rh(1)-O(12) 159.2(2), C(12)-Rh(1)-O(12) 160.5(2), C(16)-Rh(1)-O(12) 86.73(17), O(11)-Rh(1)-O(12) 90.31(14), C(15)-Rh(1)-O(12) 87.10(19).

crystal structure of **11** shows the expected square-planar coordination environment for Rh, and confirms that DMSO is bound through the oxygen atom.[26] It is worth noting that the O-bonding of DMSO leads to a significant lengthening of the S=O bond relative to free DMSO (1.536(3) and 1.528(4) Å; free DMSO: S=O 1.493(av) Å).

We prepared the first cationic, all DMSO-stabilized Rh^I complex by treating a toluene slurry of $[Rh(coe)_2(O{=}CMe_2)_2]PF_6$ with excess DMSO (Scheme 4).[27] Subsequent precipitation in diethyl ether gave $[Rh(DMSO)_2(DMSO)_2]PF_6$ (**12**) as a yellow powder in 95 % yield. The ^1H NMR spectrum of **12** in [D$_2$]dichloromethane at $-20\,^\circ C$ shows two sharp signals at 3.11 ppm (S-bound DMSO) and 2.71 ppm (O-bound DMSO); the latter signal appears as a broad singlet at room temperature. Interestingly, upon addition of two equivalents of DMSO to a solution of $[Rh(coe)_2(O{=}CMe_2)_2]PF_6$ in CD_3NO_2, only the COE ligands were displaced to give, most probably, $[Rh(DMSO)_2(O{=}CMe_2)_2]PF_6$. Treatment of complex **12** with one equivalent of 4,4′-dimethyl-2,2′-bipyridine resulted in selective substitution of the O-bound DMSO molecules to give

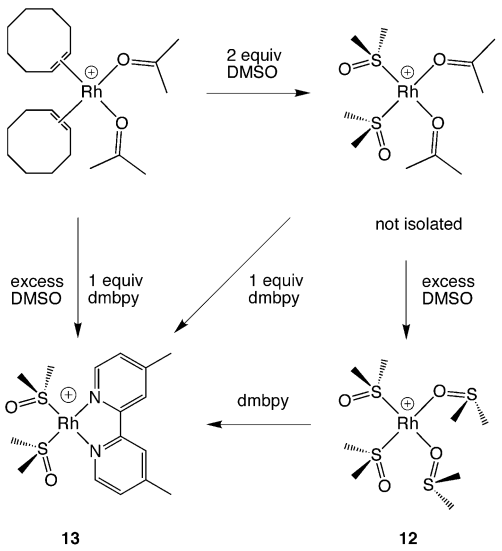

Scheme 4.

$[Rh(dmbpy)(DMSO)_2]PF_6$ (**13**) (Scheme 4). X-ray crystallographic analysis of **12** confirmed that two of the DMSO ligands are bound through the sulfur atom, while the other two DMSO molecules are bound through the oxygen atom (Figure 5), as opposed to compound **1** in which all the DMSO

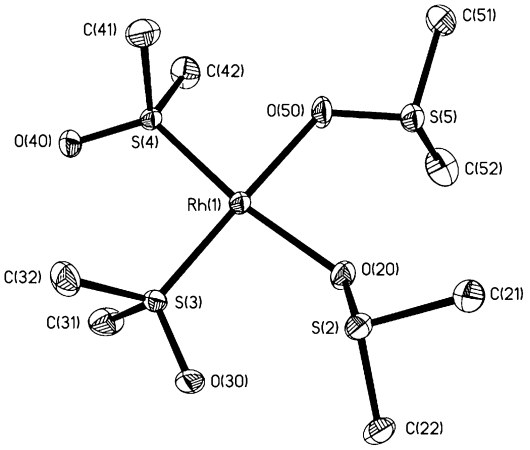

Figure 5. ORTEP drawing of complex **12**. Thermal ellipsoids are drawn at the 50 % probability level. The PF_6^- counterion and hydrogen atoms have been omitted for clarity. Selected bond lengths [Å] and angles [°]: Rh(1)–O(50) 2.099(3), Rh(1)–O(20) 2.112(3), Rh(1)–S(3) 2.1627(9), Rh(1)–S(4) 2.1643(10), S(2)–O(20) 1.539(3), S(3)–O(30) 1.494(3), S(4)–O(40) 1.486(3), S(5)–O(50) 1.530(3), O(50)-Rh(1)-O(20) 85.39(11), O(50)-Rh(1)-S(3) 178.90(10), O(20)-Rh(1)-S(3) 93.57(8), O(50)-Rh(1)-S(4) 86.14(9), O(20)-Rh(1)-S(4) 171.39(8), S(3)-Rh(1)-S(4) 94.89(4).

ligands are S-bound. As expected, binding through the oxygen atom is preferred with the harder cationic metal center. The S-bound molecules in **12** exhibit significantly shorter Rh–S bond lengths relative to those in the neutral complex **1** (2.1627(9) and 2.11643(10) Å). This can be explained by the more favorable arrangement that occurs when the O-bound DMSO molecules are *trans* to the S-bound molecules and is also reflected in the sharp signals observed in the ^1H NMR spectrum of this complex. Indeed, the O-bound DMSO is expected to have a significantly weaker *trans* influence

relative to the S-bound DMSO. The Rh–O distances are in the same range as those seen for **11** (2.112(3) and 2.099(3) Å), as is the lengthening of the S=O bond in the O-bound DMSO ligands (1.539(3) and 1.530(3) Å).

Treatment of a solution of the iridium complex $[Ir(coe)_2(O{=}CMe_2)_2]PF_6$[28] in acetone with ten equivalents of DMSO most probably affords the corresponding $[Ir(DMSO)_2(DMSO)_2]PF_6$ complex, although isolation of the pure product proved to be exceedingly difficult. When the reaction was performed under different conditions (i.e., varying the number of equivalents of DMSO), workup in diethyl ether invariably gave a yellow-brown solid. The ^{1}H NMR spectrum ([D$_6$]acetone) of the resulting solid showed the signals expected for the postulated $[Ir(DMSO)_2(DMSO)_2]PF_6$ (with signals at 3.65, 3.59, 3.21, and 3.18 ppm), but different batches were always contaminated with varying degrees of unknown by-products. In situ analysis of the bright yellow reaction solution in deuterated solvents showed that both COE molecules had been displaced. Another strong indication for its structure is the fact that substitution of the O-bound DMSO ligands by the stronger pyridine ligands (excess pyridine) gives the isolable complex $[Ir(DMSO)_2(py)_2]PF_6$ (**14**) (Scheme 5). The ^{1}H NMR spectrum of **14** in [D$_2$]dichloromethane displays one signal at 3.23 ppm, which corresponds to the S-bound DMSO ligands,

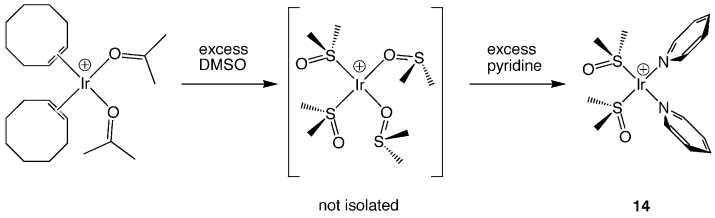

Scheme 5.

and the expected aromatic pattern for the pyridine ligands. Complete characterization of complex **14** included elemental and X-ray crystallographic analysis. Pale yellow crystals suitable for X-ray analysis were obtained by slow diffusion of diethyl ether into a concentrated solution of **14** in dichloromethane. An ORTEP diagram of **14** is shown in Figure 6, together with selected bond lengths and angles. As expected, compound **14** displays a square-planar geometry around the metal, with Ir–S bond lengths of 2.1870(14) and 2.2033(14) Å. These relatively short bond lengths (compared to **2**) indicate that the DMSO is strongly bound to the metal center, due to favorable *trans* arrangement with respect to the pyridine ligands. It should be noted that the torsion angles of the two pyridine ligands show only a slight deviation from each other (N(3)-Ir(1)-N(2)-C(25) = 99.5(4)°, N(2)-Ir(1)-N(3)-C(35) = 91.3(4)°). This means that both pyridine rings are almost perpendicular to the plane defined by the geometry around the iridium atom. The Ir–N distances of 2.076(4) and 2.102(5) Å are comparable to those found in the homogeneous hydrogenation catalyst $[Ir(cod)(py)(PCy_3)]PF_6$ (Crabtree's catalyst, Ir–N = 2.089(2) Å),[29] and are almost identical to the bond lengths found for $[Ir(cod)(py)_2]BPh_4$

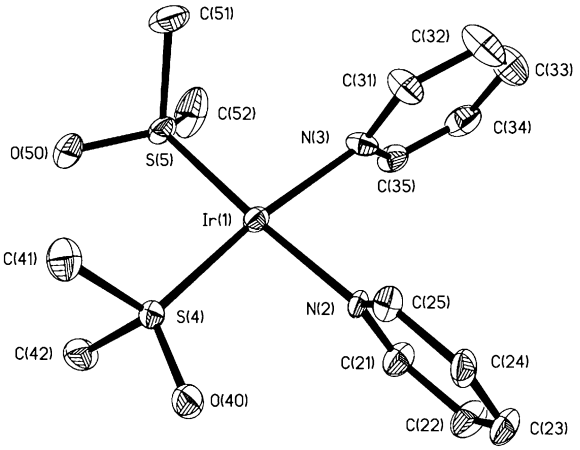

Figure 6. ORTEP drawing of complex **14**. Thermal ellipsoids are drawn at the 50 % probability level. The PF_6^- counterion and hydrogen atoms have been omitted for clarity. Selected bond lengths [Å] and angles [°]: Ir(1)–N(2) 2.076(4), Ir(1)–N(3) 2.102(5), Ir(1)–S(5) 2.1870(14), Ir(1)–S(4) 2.2033(14), S(4)–O(40) 1.484(4), S(5)–O(50) 1.480(4), N(2)-Ir(1)-N(3) 83.60(18), N(2)-Ir(1)-S(5) 176.44(12), N(3)-Ir(1)-S(5) 92.85(14), N(2)-Ir(1)-S(4) 88.37(13), N(3)-Ir(1)-S(4) 171.83(13), S(5)-Ir(1)-S(4) 95.16(6).

(2.084(8) and 2.103(8) Å).[30] As in the case of complex **5**, this once again suggests that the *trans* influence of the S-bound DMSO and that of the double bonds in COD is comparable.

Oxidative addition of X–H bonds (X = H, OH, OCH$_3$) to Ir^I DMSO complexes: Oxidative addition processes are crucial if metal complexes are to be used in catalytic transformations. We first investigated the oxidative addition of the nonpolar dihydrogen molecule to $[IrCl(DMSO)_3]$ (**2**). Indeed, when hydrogen is bubbled through a solution of **2** in [D$_6$]acetone, the intense lemon-yellow color fades to give a pale yellow solution. The ^{1}H NMR spectrum, which has three sharp signals for the S-bound DMSO ligands (at 3.26, 3.37, and 3.70 ppm), and one singlet peak at −16.11 ppm for both the hydride ligands, indicates that only one of the two possible *cis*-dihydride isomers, namely *fac*-$[Ir(H)_2Cl(DMSO)_3]$ (**15**), is formed[31] (Scheme 6). Interestingly, when the solution is left

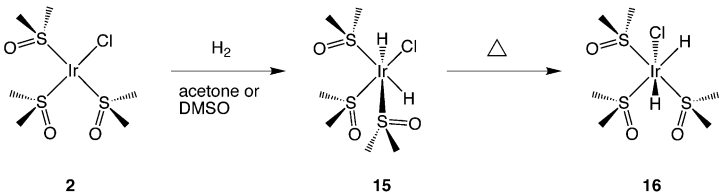

Scheme 6.

at room temperature for one day and the spectrum is re-measured, two doublet peaks for the hydrides of *mer*-$[Ir(H)_2Cl(DMSO)_3]$ (**16**) appear at −16.37 and −19.68 ppm (J = 5.8 Hz) (ratio of **15**/**16** is ca. 1:4). This shows that complex **16** is the thermodynamic product of the reaction, while **15** is the kinetic product of *cis*-oxidative addition of hydrogen. Indeed, heating a solution of **15** for 30 min at 60 °C leads to the exclusive formation of complex **16**, with a new set of signals at δ = 3.30, 3.45, and 3.53 ppm for the DMSO ligands. It should be noted that an almost identical reaction rate was

observed for the addition of hydrogen to a neat solution of **2** in DMSO;[32] this suggests that oxidative addition of hydrogen occurs directly on the 16-electron complex $[IrCl(DMSO)_3]$ (**2**), that is, without prior dissociation of DMSO. Reaction stereochemistry shows that for complex **2**, hydrogen adds preferentially along the S-Ir-S axis to yield the *cis*-dihydride product **15**, in which both hydrides are *trans* to an S-bound DMSO molecule. Since oxidative addition of H_2 is a concerted process, the activation energy for this pathway must be lower that for addition along the S-Ir-Cl axis (which would lead to **16**). This is probably due to the electronically less favorable *trans* disposition of the DMSO ligands (as compared to the DMSO ligands that are *trans* to Cl) in the starting complex **2**. Interestingly, the *trans* disposition of DMSO ligands is found in the thermodynamic product obtained from the oxidative addition of hydrogen, that is, in complex **16**. This can be explained by the *trans* influence of the different ligands, in which the chloride ligand (poorest σ-donor) prefers to be *trans* to the best σ-donor (hydride). It is worth noting that similar reactivity and stereochemistry towards oxidative addition of dihydrogen has been observed for other Ir^I phosphine complexes, such as *trans*-$[IrCl(CO)(PPh_3)_2]$ (Vaska's complex),[33] $[IrCl(CO)(dppe)]$,[34] and $[IrCl(PMe_3)_3]$.[6o]

We subsequently investigated the reactivity of **2** towards oxidative addition of polar molecules. In this context, oxidative addition of the OH bonds of water is difficult to achieve, and the relatively few examples reported involve phosphine complexes.[6] Surprisingly, addition of excess water (9 equivalents) to a yellow acetone slurry of **2** afforded pale yellow crystals of *syn*-$[(DMSO)_2HIr(\mu\text{-}OH)_2(\mu\text{-}Cl)IrH(DMSO)_2][IrCl_2(DMSO)_2]$ (**17**) within two hours. Starting from **3**, the formation of **17** was much slower and required two days for completion (Scheme 7). In both cases, analytically pure crystals of **17** were obtained in high yield. Complex **17** was also generated when a suspension of **2** in toluene was treated with five equivalents of H_2O. The ^1H NMR spectrum shows the expected hydride peak at -20.19 ppm, and three singlets between 3.39 and 3.56 ppm for the coordinated DMSO. An additional broad resonance at 5.27 ppm might be attributable to the bridging hydroxo ligand. The formulation of **17** is also supported by IR and elemental analysis. The striking difference in the reactivity of **2** and **3** towards oxidative addition of H_2O may indicate that the oxidative addition process proceeds through the 14-electron species $[IrCl(DMSO)_2]$, which is expected to be more easily generated from **2** than from **3**. Another indication that the reaction pathway involves a 14-electron intermediate stems from the fact that the addition of water to **2** is retarded by excess DMSO, and does not occur in a neat DMSO solution at room temperature. Further confirmation for the putative reaction pathway is the fact that complexes $[IrCl(py)(DMSO)_2]$ (**7**) and $[IrCl(iPr_3P)(DMSO)_2]$ (**8**) did not show any activity towards oxidative addition of H_2O at room temperature.[35] Surprisingly, when **17** was dissolved in $[D_5]$pyridine, the ^1H NMR spectrum of the resulting solution exhibited two sharp peaks at 3.61 and 3.70 ppm for the DMSO ligands, and a singlet at 4.94 ppm attributable for the free H_2O, but no hydride ligands were detected. Thus, complex **17** readily undergoes reductive elimination in pyridine. Both NMR spectroscopic data and elemental analysis of the non-deuterated complex show that the known complex $[IrCl(py)(DMSO)_2]$ (**7**) was formed (see discussion above).

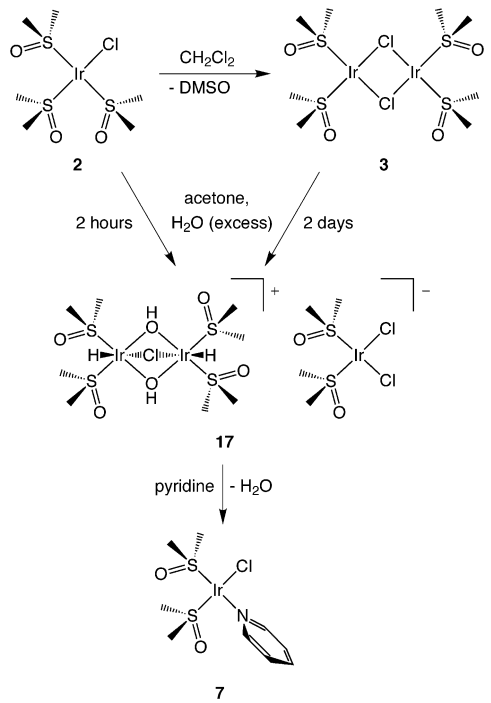

Scheme 7.

Crystals of complex **17** suitable for X-ray crystallography were grown from a dilute solution of **2** (or **3**) in acetone/water. An ORTEP view with selected bond lengths and angles is shown in Figure 7, and reveals that the cationic part of the hydrido–hydroxo complex has a dinuclear structure in which each iridium atom is located in a highly distorted octahedral environment. The iridium atoms are bound to two DMSO molecules through the sulfur atom, and are bridged by a Cl atom and two hydroxo ligands. The terminal hydride ligands were not located, but their position is inferred to be *trans* to the μ-chloro ligand and *cis* to the hydroxo bridges. Closely related derivatives of such a triply-bridged dinuclear structure are the methoxy-bridged $[(binap)HIr(\mu\text{-}OMe)_2(\mu\text{-}Cl)IrH(binap)]Cl$,[6m] and the mixed complex $[(Et_3P)_2HIr(\mu\text{-}OH)(\mu\text{-}Cl)(\mu\text{-}NHPh)IrH(PEt_3)_2]Cl$.[36] The counteranion for complex **17** consists of a unique $[IrCl_2(DMSO)_2]^-$ fragment, which has a distorted square-planar configuration. Not surprisingly, the Ir–S bond lengths in this anionic species are slightly shorter (2.174(8) and 2.180(8) Å) than those found in the cationic part of complex **17** (2.207(av) Å).

Oxidative addition of water to the cationic iridium(I) system was also studied. As described above, when ten equivalents of DMSO were added to a solution of $[Ir(coe)_2(O{=}CMe_2)_2]PF_6$ in acetone, the DMSO complex $[Ir(DMSO)_2(DMSO)_2]PF_6$ was most probably formed. Subsequently, in situ treatment of this complex with excess water led to the clean oxidative addition and isolation of the cationic complex *anti*-$[(DMSO)_2(DMSO)HIr(\mu\text{-}OH)_2IrH(DMSO)_2(DMSO)][PF_6]_2$ (**18**) in high yield (Scheme 8). As in the case of **17**, character-

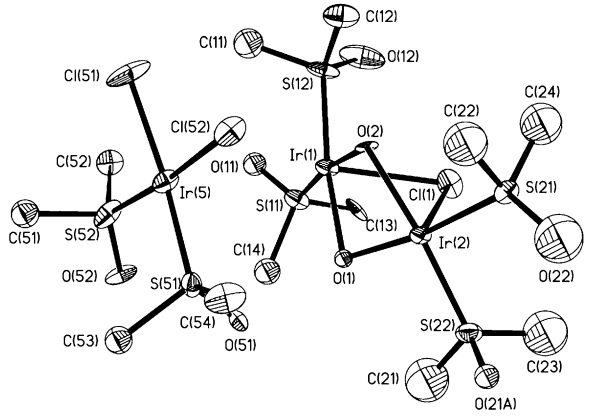

Figure 7. ORTEP plot of a molecule of **17**. Thermal ellipsoids are drawn at the 50% probability level. Hydrogen atoms and solvent molecules have been omitted for clarity. Selected bond lengths [Å] and angles [°]: Ir(1)–O(1) 2.054(17), Ir(1)–O(2) 2.100(17), Ir(1)–S(11) 2.197(8), Ir(1)–S(12) 2.211(7), Ir(1)–Cl(1) 2.661(8), Ir(1)···Ir(2) 3.0277(17), Ir(2)–O(1) 2.055(17), Ir(2)–O(2) 2.070(17), Ir(2)–S(22) 2.201(8), Ir(2)–S(21) 2.219(8), Ir(2)–Cl(1) 2.510(7), Ir(5)–S(52) 2.174(8), Ir(5)–S(51) 2.180(8), Ir(5)–Cl(51) 2.359(8), Ir(5)–Cl(52) 2.403(8), S(11)–O(11) 1.49(2), S(12)–O(12) 1.47(3), S(21)–O(22) 1.43(3), S(22)–O(21A, 21B) 1.45, S(51)–O(51) 1.49(2), S(52)–O(52) 1.47(2), O(1)-Ir(1)-O(2) 79.2(7), S(11)-Ir(1)-S(12) 93.0(3), O(1)-Ir(1)-Cl(1) 75.1(5), O(2)-Ir(1)-Cl(1) 74.0(5), S(11)-Ir(1)-Cl(1) 101.5(3), S(12)-Ir(1)-Cl(1) 98.4(3), O(1)-Ir(2)-O(2) 79.8(7), S(22)-Ir(2)-S(21) 93.5(3), O(1)-Ir(2)-Cl(1) 78.6(5), O(2)-Ir(2)-Cl(1) 77.9(5), S(22)-Ir(2)-Cl(1) 101.2(3), S(21)-Ir(2)-Cl(1) 98.0(3), Ir(2)-Cl(1)-Ir(1) 71.6(2), Ir(1)-O(1)-Ir(2) 94.9(7), Ir(2)-O(2)-Ir(1) 93.1(7), S(52)-Ir(5)-S(51) 92.1(3), S(52)-Ir(5)-Cl(51) 88.2(3), S(51)-Ir(5)-Cl(51) 173.5(3), S(52)-Ir(5)-Cl(52) 174.8(3), S(51)-Ir(5)-Cl(52) 92.4(3), Cl(51)-Ir(5)-Cl(52) 86.9(3).

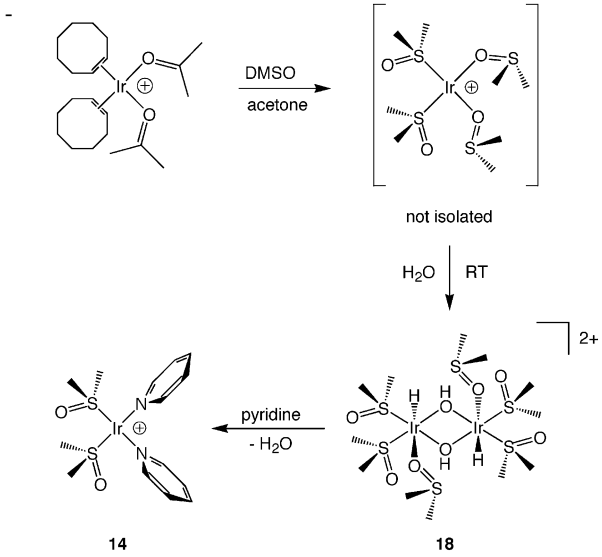

Scheme 8.

ization of **18** by NMR spectroscopy was hampered by its low solubility in common organic solvents. The ^{1}H NMR spectrum in a [D_6]acetone/[D_6]DMSO mixture exhibits the hydride peak at −24.74 ppm, and as expected, the O-bound DMSO ligand appears at higher field (3.13 ppm) relative to the S-bound ligand (3.40 and 3.48 ppm). A broad signal at 4.03 ppm can be attributed to the hydroxo bridges. In the IR spectrum (KBr disk), the hydride gives rise to a peak at 2213 cm^{-1}, and the hydroxo bridges appear as a broad peak at 3441 cm^{-1}. The formulation of **18** is also supported by elemental analysis, and was confirmed by X-ray crystal analysis. A plausible reaction pathway for the formation of complex **18** involves replacement of one of the O-bound DMSO ligands in [Ir(DM*S*O)$_2$(DMS*O*)$_2$]PF$_6$ with a molecule of water followed by oxidative addition. Dissolving **18** in pyridine once again led to ready reductive elimination of water and afforded the Ir^{I} compound [Ir(py)$_2$(DM*S*O)$_2$]PF$_6$ (**14**). This complex was also directly obtained by treating a solution of [Ir(coe)$_2$(O=CMe$_2$)$_2$]PF$_6$ in acetone with ten equivalents of DMSO and five equivalents of pyridine (see discussion above). As observed for the neutral pyridine complex [IrCl(py)(DM*S*O)$_2$] (**7**), oxidative addition of water to complex **14** was not observed at ambient temperature.

The ORTEP diagram for compound **18** (together with a selected list of bond lengths and angles) is shown in Figure 8. The structure displays a distorted octahedral geometry at the

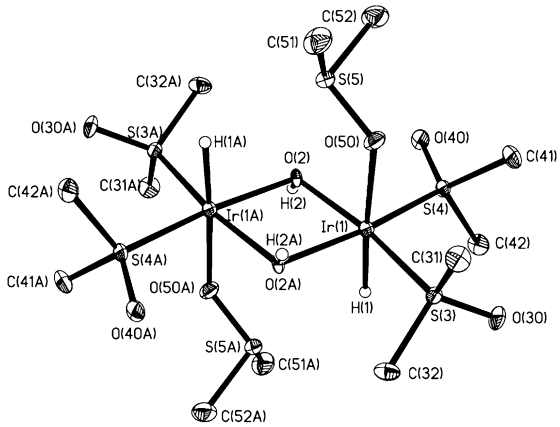

Figure 8. ORTEP view of a molecule of **18**. Thermal ellipsoids are drawn at the 50% probability level. The PF_6^- counterions, hydrogen atoms, and solvent molecules have been omitted for clarity. Selected bond lengths [Å] and angles [°]: Ir(1)–O(2) 2.074(3), Ir(1)–O(1A) 2.093(3), Ir(1)–S(3) 2.2077(13), Ir(1)–S(4) 2.2142(12), Ir(1)–O(50) 2.218(3), Ir(1)–H 1.66(9), Ir(1)···Ir(1A) 3.235, S(3)–O(30) 1.477(3), S(4)–O(40) 1.477(4), S(5)–O(50) 1.542(3), O(2)-Ir(1)-O(2A) 78.12(15), O(2)-Ir(1)-S(3) 171.32(9), O(2A)-Ir(1)-S(3) 93.20(10), O(2)-Ir(1)-S(4) 93.17(10), O(2A)-Ir(1)-S(4) 171.06(10), S(3)-Ir(1)-S(4) 95.49(5), O(2)-Ir(1)-O(50) 86.86(14), O(2A)-Ir(1)-O(50) 91.67(14), S(3)-Ir(1)-O(50) 93.67(10), S(4)-Ir(1)-O(50) 89.85(10), O(2)-Ir(1)-H(1) 97(3), O(2A)-Ir(1)-H(1) 90(3), S(3)-Ir(1)-H(1) 83(3), S(4)-Ir(1)-H(1) 89(3).

Ir^{III} centers, with two bridging hydroxo ligands and terminal hydrides. Interestingly, the DMSO ligands exhibit two coordination modes in the same molecule. Each iridium atom is coordinated to two DMSO molecules through the sulfur atoms and to one DMSO molecule through the oxygen atom. This is the first iridium complex characterized by crystallography to exhibit O-bonding of a sulfoxide ligand. As seen in O-bonding to rhodium, a substantially longer S=O distance (1.542(3) Å) is observed relative to the values found for free DMSO. It should be noted that the hydride is located *trans* to the O-bound DMSO. The Ir–S bond lengths are similar to those found in the Ir^{I} complex **14** (2.2077(13) and 2.2142(12) Å for **18**; 2.1870(14) and 2.2033(14) Å for **14**).

Finally, we were also interested in determining whether the complexes in our study undergo oxidative addition of MeOH.

Reaction of solutions of the neutral complexes **2** and **3** in acetone with excess MeOH afforded a yellow solution from which neither clean nor isolable products were obtained. In contrast, when a solution of $[Ir(coe)_2(O{=}CMe_2)_2]PF_6$ in methanol was treated with a slight excess of DMSO and was was left to stand at room temperature for two days, pale yellow crystals formed, which were subjected to X-ray crystallography. To our surprise, besides isolating the new complex *syn*-$[(DMSO)_2HIr(\mu\text{-}OCH_3)_3IrH(DMSO)_2]PF_6$ (**19**), the crystalline material also contained substantial amounts of complex **18** (Scheme 9). Therefore, it seems that although the

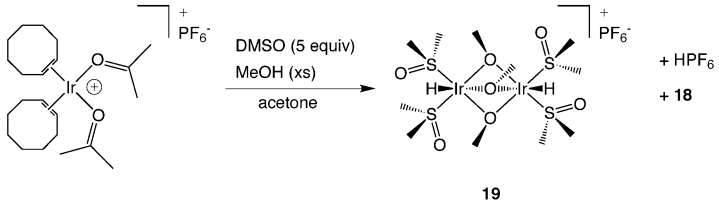

Scheme 9.

work was carried out under strictly anhydrous conditions, traces of water present in the system led to the formation of **18**. This phenomenon was also observed when a solution of $[Ir(coe)_2(O{=}CMe_2)_2]PF_6$ in acetone was treated with five equivalents of DMSO and five equivalents of MeOH. Unfortunately, the color and shape of the crystals obtained were identical and precluded any mechanical separation of **18** and **19**, and we were, therefore, unable to characterize compound **19** by spectroscopic methods.[37] Although frustrating, this result nevertheless demonstrates the extraordinary affinity of this system towards oxidative addition of water over MeOH. An ORTEP drawing of complex **19** with selected bond lengths and angles is shown in Figure 9. Interestingly, the structure for compound **19** is not analogous to complex **18**. Although it shows a similar dimeric structure in which both Ir^{III} centers display a distorted octahedral geometry, the two metal centers are triply bridged by three methoxy ligands. This means that the dimer is monocationic with three terminal ligands per iridium, namely two DMSO molecules coordinated through sulfur atoms and a terminal hydride, which was not located but its position is inferred to be *trans* to the methoxy bridge O(5)–C(5), as it displays substantially longer Ir–O distances than the other two methoxy units.[38] The Ir–S bond lengths in this complex (2.229(av) Å) are similar to the values observed for **17** and **18**.

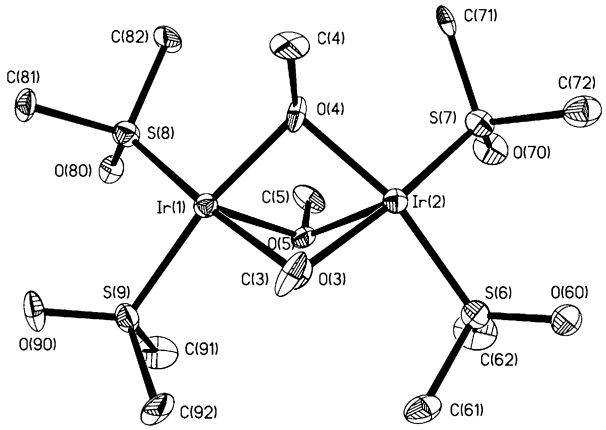

Figure 9. ORTEP plot of a molecule of **19**. Thermal ellipsoids are drawn at the 50% probability level. The PF_6^- counterion, hydrogen atoms, and solvent molecules have been omitted for clarity. Selected bond lengths [Å] and angles [°]: Ir(1)–O(4) 2.038(11), Ir(1)–O(3) 2.062(10), Ir(1)–O(5) 2.158(10), Ir(1)–S(8) 2.237(4), Ir(1)–S(9) 2.243(4), Ir(1)···Ir(2) 2.9906(10), Ir(2)–O(4) 2.062(11), Ir(2)–O(3) 2.075(11), Ir(2)–S(7) 2.208(4), Ir(2)–O(5) 2.224(11), Ir(2)–S(6) 2.228(4), O(3)–C(3) 1.445(18), O(4)–C(4) 1.451(17), O(5)–C(5) 1.471(17), S(6)–O(60) 1.466(12), S(7)–O(70) 1.507(11), S(8)–O(80) 1.491(11), S(9)–O(90) 1.470(10), O(4)-Ir(1)-O(3) 77.8(4), O(4)-Ir(1)-O(5) 75.6(4), O(3)-Ir(1)-O(5) 72.7(4), O(4)-Ir(1)-S(8) 98.0(3), O(3)-Ir(1)-S(8) 173.9(3), O(5)-Ir(1)-S(8) 102.0(3), O(4)-Ir(1)-S(9) 170.2(3), O(3)-Ir(1)-S(9) 94.8(3), O(5)-Ir(1)-S(9) 96.1(3), S(8)-Ir(1)-S(9) 88.87(14), O(4)-Ir(2)-O(3) 77.0(4), O(4)-Ir(2)-S(7) 97.6(3), O(3)-Ir(2)-S(7) 173.2(3), O(4)-Ir(2)-O(5) 73.7(4), O(3)-Ir(2)-O(5) 71.1(4), S(7)-Ir(2)-O(5) 103.5(3), O(4)-Ir(2)-S(6) 165.9(3), O(3)-Ir(2)-S(6) 92.5(3), S(7)-Ir(2)-S(6) 92.12(14), O(5)-Ir(2)-S(6) 94.2(3).

Conclusion

In summary, we have reported the synthesis, isolation, and characterization of the first neutral and cationic Rh^I and Ir^I complexes that have only DMSO molecules as dative ligands. These complexes can be obtained quantitatively from Rh^I and Ir^I olefin precursors. The X-ray crystal structures of the neutral derivatives $[RhCl(DMSO)_3]$ and $[IrCl(DMSO)_3]$ show that all the DMSO molecules are bound through the sulfur atom. With the harder metal center in the cationic systems, both S- and O-bonding are involved, as shown by X-ray crystallography of the rhodium compound $[Rh(DMSO)_2(DMSO)_2]PF_6$. In addition, the first example of a square-planar bimetallic complex with a bidentate S,O-bridging DMSO ligand was characterized, and was shown by X-ray crystallography to be [(coe)(DMSO)Rh(μ-Cl)(μ-DMSO)RhCl(DMSO)]. All of the above complexes were obtained from M^I–COE (M = Rh, Ir) precursors. Metal precursors that contained chelating olefins (i.e., M^I–COD complexes) generated, upon reaction with DMSO, mixed COD–DMSO complexes; this indicates that substitution of a chelating olefin with DMSO is much more difficult.

Reaction of DMSO-stabilized neutral complexes with pyridine led to substitution of only one of the DMSO ligands, whereas the bidentate dmbpy ligand displaced two of them. Reaction of these two ligands with the cationic DMSO complexes led to the selective substitution of the O-bound ligands. In all these cases, the resultant mixed ligand systems were shown to be stable towards further ligand dissociation.

The neutral iridium complex $[IrCl(DMSO)_3]$ underwent oxidative addition of dihydrogen to give, in a first step, the kinetic species, which was subsequently easily converted to the more stable thermodynamic product. Surprisingly, both neutral and cationic Ir^I–DMSO complexes can easily activate the polar O–H bond of water at room temperature to give the novel hydrido–hydroxo complexes **17** and **18**, respectively, in good yield. X-ray crystallographic studies determined that both compounds have dinuclear structures, and in complex **18** both O- and S-bound DMSO ligands are present. Reductive elimination of water from **17** and **18** in pyridine leads to

quantitative isolation of the mixed Ir^I–DMSO–pyridine complexes **7** and **14**, respectively. The cationic Ir^I–DMSO complex underwent oxidative addition of MeOH to afford the monocationic hydrido–methoxo complex **19**, which was characterized by crystallography.

Thus, we have shown that nontoxic and inexpensive DMSO can be used as an effective ligand for stabilizing low-valent Ir^I and Rh^I species. Moreover, we believe that the reactivity patterns described herein will pave the way for future catalytic applications of such compounds.

Experimental Section

General procedures: All experiments were carried out under an atmosphere of purified nitrogen in a Vacuum Atmospheres glove box. All solvents were reagent grade or better. Dimethylsulfoxide (anhydrous) was purchased from Aldrich, degassed with argon, and dried over molecular sieves. $[Ir_2Cl_2(cod)_2]$ was purchased from Strem Chemicals. All nondeuterated solvents were refluxed over sodium benzophenone ketyl and distilled under an argon atmosphere. Deuterated solvents were used as received. All the solvents were degassed with argon and kept over molecular sieves in the glove box. Commercially available reagents were used as received. Work with $AgPF_6$ was performed in the absence of light. The complexes $[Rh_2Cl_2(coe)_4]$,[39] $[Rh_2Cl_2(cod)_2]$,[40] $[Rh(cod)_2]BF_4$,[41] $[Rh(coe)_2(O{=}CMe_2)_2]PF_6$,[27] $[Ir_2Cl_2(coe)_4]$,[42] and $[Ir(coe)_2(O{=}CMe_2)_2]PF_6$,[28] were prepared according to literature procedures.

^{1}H NMR spectra were recorded on Bruker DPX-250 or Bruker DRX-400 spectrometers. NMR chemical shifts are reported in ppm downfield from tetramethylsilane, and the residual solvent peak was used as the reference. Abbreviations used in the description of NMR data are as follows: br, broad; s, singlet; m, multiplet. FT-IR spectra were recorded on a Nicolet PROTEGE 460 spectrometer. Elemental analyses were performed by H. Kolbe, Mikroanalytisches Laboratorium, 45470 Mühlheim, Germany.

[RhCl(DMSO)$_3$] (1): Dropwise addition of DMSO (1 mL) to an orange suspension of $[Rh_2Cl_2(coe)_4]$ (350 mg, 0.489 mmol) in toluene (8 mL) afforded a limpid yellow-orange solution. Stirring at room temperature for 3 h resulted in the fomration of a yellow-orange precipitate formed, which was filtered off, washed with diethyl ether, and dried under vacuum. Crystals of **1** suitable for X-ray diffraction were obtained by leaving $[Rh_2Cl_2(coe)_4]$ (60 mg) in a mixture of toluene (3 mL) and DMSO (0.6 mL). Yield 328 mg (90 %); ^{1}H NMR (CD_2Cl_2): $\delta = 3.19$ ppm (br s, 18 H); elemental analysis calcd (%) for $C_6H_{18}ClO_3RhS_3$: C 19.33, H 4.87; found: C 19.24, H 4.81.

[IrCl(DMSO)$_3$] (2): Dropwise addition of DMSO (1 mL) to a bright orange suspension of $[Ir_2Cl_2(coe)_4]$ (438 mg, 0.489 mmol) in toluene (8 mL) afforded a limpid yellow-orange solution. Stirring at at room temperature for 3 h, resulted in the formation of a bright yellow precipitate, which was filtered off, washed with diethyl ether, and dried under vacuum. Crystals of **2** suitable for X-ray diffraction were obtained by leaving $[Ir_2Cl_2(coe)_4]$ (100 mg) in a mixture of toluene (4 mL) and DMSO (1 mL). Yield 406 mg (90 %); ^{1}H NMR ([D$_6$]acetone): $\delta = 2.70$–3.80 ppm (shoulder, 18 H); elemental analysis calcd (%) for $C_6H_{18}ClIrO_3S_3$: C 15.60, H 3.93; found: C 15.59, H 4.06.

[Ir$_2$Cl$_2$(DMSO)$_4$] (3): Complex **2** (102 mg, 0.221 mmol) was dissolved in a minimum amount of CH_2Cl_2 (8 mL). The resulting red solution was stirred at room temperature for 3 h. Addition of diethyl ether (20 mL) afforded an orange-red solid, which was filtered off, washed with additional diethyl ether, and dried under vacuum. Yield 80 mg (95 %); ^{1}H NMR (CD_2Cl_2): $\delta = 3.47$ (br s, 12 H), 3.64 ppm (br s, 12 H); elemental analysis calcd (%) for $C_8H_{24}Cl_2Ir_2O_4S_4$: C 12.51, H 3.15; found: C 12.45, H 3.09.

[(coe)(DMSO)Rh(μ-Cl)(μ-DMSO)RhCl(DMSO)] (4): A solution of DMSO (46 mg, 0.587 mmol) in toluene (1 mL) was added to a bright orange suspension of $[Rh_2Cl_2(coe)_4]$ (70 mg, 0.098 mmol) in toluene (8 mL) to give a limpid yellow-orange solution, which was left to stand in a high-walled flask for 2 days. The crystals obtained were collected, washed with diethyl ether, and dried under vacuum. X-ray quality crystals were obtained in a similar manner. Yield 27 mg (45 %); ^{1}H NMR (CD_2Cl_2): $\delta = 1.56$ (br m, 8 H), 1.96 (br m, 2 H), 2.31 (br m, 2 H), 3.14–3.30 (several br s, 18 H), 3.82 ppm (m, 2 H); elemental analysis calcd (%) for $C_{14}H_{32}Cl_2O_3RhS_3$: C 27.06, H 5.19; found: C 27.85, H 5.23.

[IrCl(cod)(DMSO)] (5): Addition of DMSO (110 mg, 1.408 mmol) to a bright orange suspension of $[Ir_2Cl_2(cod)_2]$ (220 mg, 0.328 mmol) in toluene (4 mL) gave a limpid yellow solution, which was stirred at room temperature for 2 h. The solution was then poured into diethyl ether/pentane (1:3, 50 mL) to give a yellow precipitate. This was filtered off, washed with pentane, and dried under vacuum. Crystals of **5** suitable for X-ray diffraction were obtained by slow evaporation of a diethyl ether solution of **5**. Yield 117 mg (86 %); ^{1}H NMR (C_6D_6): $\delta = 1.76$ (m, 8 H), 2.96 (s, 6 H), 4.00 (m, 2 H), 5.00 ppm (m, 2 H); elemental analysis calcd (%) for $C_{10}H_{18}ClIrOS$: C 29.01, H 4.39; found: C 29.13, H 4.39.

[RhCl(py)(DMSO)$_2$] (6): A solution of pyridine (74 mg, 0.939 mmol) in benzene (2 mL) was added dropwise to an orange suspension of [RhCl(DMSO)$_3$] (**1**) (70 mg, 0.188 mmol) in benzene (5 mL). The resulting yellow suspension was stirred at room temperature for 2 h, during which time the suspension turned almost limpid. Addition of diethyl ether (7 mL) and pentane (5 mL) afforded a yellow-green precipitate, which was washed with diethyl ether and dried under vacuum. Yield 60 mg (86 %); ^{1}H NMR (C_6D_6): $\delta = 3.01$ (s, 6 H), 3.03 (s, 6 H), 6.33 (dd, $J = 6.5$ Hz, 2 H), 6.60 (dd, $J = 7.7$ Hz, 1 H), 8.78 ppm (d, $J = 4.9$ Hz, 2 H); elemental analysis calcd (%) for $C_9H_{17}ClNO_2RhS_2$: C 28.92, H 4.59, N 3.75; found: C 28.78, H 4.48, N 3.87.

[IrCl(py)(DMSO)$_2$] (7): Pyridine (2 mL) was added to a red solution of **2** (235 mg, 0.334 mmol) in dichloromethane (9 mL), and the solution was stirred at room temperature for 1 h, during which time the solution turned yellow. The solution was then concentrated to 4 mL. Addition of a diethyl ether/pentane mixture afforded an off-white solid. The solid was filtered, washed with additional diethyl ether, and dried under vacuum. Yield 195 mg (75 %). ^{1}H NMR (CD_2Cl_2): $\delta = 3.40$ (s, 6 H), 3.48 (s, 6 H), 7.30 (m, 2 H), 7.75 (m, 1 H), 8.73 ppm (m, 2 H); elemental analysis calcd (%) for $C_9H_{17}ClIrNO_2S_2$: C 23.34, H 3.70, N 3.03; found: C 22.37, H 3.30, N 3.15.

[IrCl(*i*Pr$_3$P)(DMSO)$_2$] (8): A solution of triisopropylphosphine (48.6 mg, 0.302 mmol) in pentane (0.5 mL) was added to a lemon-yellow suspension of **2** (70 mg, 0.151 mmol) in a mixture of pentane (1.5 mL) and benzene (0.75 mL). The resulting suspension was then stirred at room temperature, during which time it turned bright yellow. The suspension was cooled to $-30\,^\circ$C for 2 h, decanted, washed with small amounts of cold pentane ($-30\,^\circ$C), and dried under vacuum. Yield 62 mg (75 %); ^{31}P NMR (C_6D_6): $\delta = 34.24$ ppm (s, 1 P); ^{1}H NMR (C_6D_6): $\delta = 1.34$ (q, 18 H), 2.91 (s, 6 H), 3.09 (m, 3 H), 3.40 ppm (s, 6 H); elemental analysis calcd (%) for $C_{13}H_{33}ClIrO_2PS_2$: C 28.69, H 6.12; found: C 28.61, H 6.04.

[RhCl(dmbpy)(DMSO)] (9): An orange solution of complex **1** (256 mg, 0.692 mmol) in DMSO (8 mL) was stirred at room temperature for 10 min. Upon addition of dmbpy (128 mg, 0.692 mmol) in small portions, the solution turneddeep red. The solution was stirred for 3 h at room temperature and then poured into diethyl ether (250 mL). This resulted in the precipitation of a red solid, which was decanted, washed with diethyl ether and pentane, and dried under vacuum. Yield 245 mg (88 %); ^{1}H NMR ([D$_6$]acetone): $\delta = 2.31$ (s, 3 H), 2.51 (s, 3 H), 3.19 (s, 6 H), 7.16 (d, $J = 6.0$ Hz, 1 H), 7.45 (d, $J = 5.8$ Hz, 1 H), 8.03 (s, 1 H), 8.18 (s, 1 H), 9.46 (d, $J = 5.7$ Hz, 1 H), 9.83 ppm (d, $J = 6.0$ Hz, 1 H); elemental analysis calcd (%) for $C_{14}H_{18}ClN_2ORhS$: C 41.96, H 4.53, N 6.99; found: C 41.78, H 4.46, N 7.06.

[IrCl(dmbpy)(DMSO)] (10): After dmbpy (78 mg, 0.422 mmol) was added in small portions to a yellow solution of complex **2** (195 mg, 0.422 mmol) in DMSO (5 mL), the solution turned violet. The solution was stirred for 1 h at room temperature and was then poured into diethyl ether (150 mL), resulting in the precipitation of a dark violet solid; this was then decanted, washed with diethyl ether and pentane, and dried under vacuum. Yield 199 mg (83 %); ^{1}H NMR ([D$_6$]DMSO): $\delta = 1.90$ (s, 3 H), 2.44 (s, 3 H), 7.01 (d, $J = 5.5$ Hz, 1 H), 7.64 (d, $J = 5.8$ Hz, 1 H), 8.00 (s, 1 H), 8.32 (s, 1 H), 9.68 (d, $J = 5.8$ Hz, 1 H) 10.37 ppm (d, $J = 5.9$ Hz, 1 H).

[Rh(cod)(DMSO)$_2$]BF$_4$ (11): A solution of DMSO (141 mg, 1.807 mmol) in dichloromethane (1 mL) was added dropwise to a red solution of $[Rh(cod)_2]BF_4$ (37 mg, 0.090 mmol) in dichloromethane (1 mL). The resulting bright yellow solution was stirred at room temperature for 5 h, and upon addition of diethyl ether a yellow solid precipitated; this was washed with additional diethyl ether and dried under vacuum. X-ray

quality crystals were obtained from slow evaporation of a concentrated CH_2Cl_2 solution of **11**. Yield 34 mg (82%); ^{1}H NMR (CD_2Cl_2): $\delta = 1.71$ (m, 4H), 2.48 (m, 4H), 2.76 (s, 12H), 3.94 ppm (br s, 4H); elemental analysis calcd (%) for $C_{12}H_{24}BF_4O_2RhS_2$: C 31.74, H 5.33; found: C 31.62, H 5.25.

[Rh(DMSO)$_2$(DMS*O*)$_2$]PF$_6$ (12): Dropwise addition of DMSO (1 mL) to a suspension of $[Rh(coe)_2(O{=}CMe_2)_2]PF_6$ (102.0 mg, 0.175 mmol) in toluene (5 mL) gave a yellow solution, which was left to stir at room temperature for 30 min. The solution was then poured into diethyl ether (60 mL), and the resulting yellow precipitate was washed with additional diethyl ether and dried under vacuum. Crystals of **12** suitable for X-ray diffraction were obtained by slow diffusion of diethyl ether into a concentrated CH_2Cl_2 solution of **12**. Yield 93 mg (95%); ^{1}H NMR (CD_2Cl_2, 253 K): $\delta = 2.71$ (s, 12H), 3.11 ppm (s, 12H); IR (KBr): $\tilde{\nu} = 929$ cm^{-1} (s, S=*O*), 1101 (s, *S*=O); elemental analysis calcd (%) for $C_8H_{24}F_6O_4PRhS_4$: C 17.15, H 4.32; found: C 16.89, H 4.31.

[Rh(dmbpy)(DMSO)$_2$]PF$_6$ (13): Complex **12** (65 mg, 0.115 mmol) and dmbpy (21 mg, 0.115 mmol) were dissolved in DMSO (4 mL), and the resulting deep-red solution was stirred at room temperature for 2 h. The solution was then poured into diethyl ether (150 mL), and the brick-red precipitate that formed was decanted, washed with diethyl ether, and dried under vacuum. Yield 61 mg (90%); ^{1}H NMR ([D$_6$]DMSO): $\delta = 2.52$ (s, 6H), 7.52 (d, $J = 5.9$ Hz, 2H), 8.41 (s, 2H), 8.70 ppm (d, $J = 5.8$ Hz, 2H); elemental analysis calcd (%) for $C_{16}H_{24}F_6N_2O_2PRhS_2$: C 32.66, H 4.11, N 4.76; found: C 32.78, H 4.18, N 4.71.

[Ir(py)$_2$(DMSO)$_2$]PF$_6$ (14): DMSO (95 mg, 1.220 mmol) and pyridine (48 mg, 0.610 mmol) were added to an orange solution of $[Ir(coe)_2(O{=}CMe_2)_2]PF_6$ (82 mg, 0.122 mmol) in acetone (5 mL). The resulting light-yellow solution was stirred at room temperature for 1.5 h and concentrated to 3 mL. Addition of diethyl ether (10 mL) afforded an off-white solid, which was decanted, washed with diethyl ether, and dried under vacuum. Crystals suitable for X-ray diffraction were obtained by slow diffusion of diethyl ether into a concentrated CH_2Cl_2 solution of **14**. Yield 64 mg (81%). ^{1}H NMR (CD_2Cl_2): $\delta = 3.23$ (s, 12H), 7.43 (m, 4H), 7.81 (m, 2H), 8.76 ppm (m, 4H); elemental analysis calcd (%) for $C_{14}H_{22}F_6IrN_2O_2PS_2$: C 25.80, H 3.40, N 4.30; found: C 25.95, H 3.32, N 4.36.

In situ characterization of *fac*-[Ir(H)$_2$Cl(DMSO)$_3$] (15) and *mer*-[Ir(H)$_2$Cl(DMSO)$_3$] (16): Complex **2** (15.0 mg, 0.033 mmol) was dissolved in [D$_6$]acetone (1.5 mL), and the resulting yellow-orange solution was transferred to an NMR tube. A slow stream of hydrogen was then bubbled through the solution for 5 min during which time the solution turned bright yellow. After 10 min, complex **15** was quantitatively formed as revealed by ^{1}H NMR spectroscopy. ^{1}H NMR ([D$_6$]acetone): $\delta = -16.11$ (s, 2H), 3.26 (s, 6H), 3.37 (s, 6H), 3.70 ppm (s, 6H). The solution was subsequently heated for 30 min at 60 °C; this resulted in the quantitative formation of **16**. ^{1}H NMR ([D$_6$]acetone): $\delta = -19.68$ (d, $J = 5.8$ Hz, 1H), -16.37 (d, $J = 5.8$ Hz, 1H), 3.30 (s, 6H), 3.45 (s, 6H), 3.53 ppm (s, 6H).

***syn*-[(DMSO)$_2$HIr(μ-OH)$_2$(μ-Cl)IrH(DMSO)$_2$][IrCl$_2$(DMSO)$_2$] (17)**: Complex **2** (60 mg, 0.129 mmol) was dissolved in acetone (4 mL)and H_2O (20 mg) to afford a pale yellow limpid solution. Upon standing at room temperature for 2 h, large amounts of orange-yellow crystals were formed. The mother liquor was filtered and the solid was dried under vacuum for 24 h. Crystals of **17** suitable for X-ray diffraction were obtained by leaving **2** (20 mg) in acetone (4 mL) which contained H_2O (15 mg). Yield 42 mg (85%); ^{1}H NMR (CD_2Cl_2): $\delta = -20.19$ (s, 2H; Ir–H), 3.39, 3.44, 3.56 (3s, 12H each; CH_3 groups), 5.27 ppm (br s, 2H, probably Ir–OH); IR (KBr): $\tilde{\nu} = 2231$ (s, Ir–H), 3260 cm^{-1} (sh s, OH); elemental analysis calcd (%) for $C_{12}H_{40}Cl_3Ir_3O_8S_6$: C 12.13, H 3.39; found: C 11.24, H 3.58.

***anti*-[(DMSO)$_2$(DMS*O*)HIr(μ-OH)$_2$IrH(DMSO)$_2$(DMS*O*)][(PF$_6$)$_2$] (18)**: DMSO (0.5 mL) was added dropwise to a yellow-orange solution of $[Ir(coe)_2(O{=}CMe_2)_2]PF_6$ (60 mg, 0.089 mmol) in acetone (6 mL) to afford a pale yellow solution. This was then treated with H_2O (20 mg) and left to stand at room temperature for 4 h, during which time pale yellow crystals formed. Slow diffusion of diethyl ether afforded a pale yellow crystalline solid, which was dried under vacuum. Crystals of **18** suitable for X-ray diffraction were obtained in a similar manner (without final drying under vacuum). Yield 43 mg (82%); ^{1}H NMR ([D$_6$]acetone/[D$_6$]DMSO): $\delta = -24.74$ (s, 2H; Ir–H), 3.13 (s, 12H; CH_3-DMS*O*), 3.40, 3.48 (s, 12H each; CH_3-DMS*O*), 4.03 ppm (br s, 2H; probably Ir–OH); IR (KBr): $\tilde{\nu} = 2213$ (s, Ir–H), 3441 cm^{-1} (sh s, OH); elemental analysis calcd (%) for $C_6H_{20}F_6IrO_4PS_3{+}C_2H_6SO$ (solvate, see X-ray structure): C 14.39, H 3.92; found: C 13.86, H 3.82.

***syn*-[(DMSO)$_2$HIr(μ-OCH$_3$)$_3$IrH(DMSO)$_2$]PF$_6$ (19)**: A solution of $[Ir(coe)_2(O{=}CMe_2)_2]PF_6$ (60 mg, 0.148 mmol) in acetone (4 mL) was treated with DMSO (58 mg, 0.740 mmol) and MeOH (24 mg, 0.740 mmol), and was then left to stand at room temperature for 6 h. Subsequently, diethyl ether (10 mL) was layered on top and slowly diffused to afford pale yellow crystals. These contained a mixture of **18** and **19**. Yield 75 mg.

X-ray crystal structure determination of 1, 2, 4, 5, 11, 12, 14, 17, 18, and 19: Single crystals were mounted on a nylon loop in cryo-oil and flash frozen in a nitrogen stream at 120 K. Data were collected on a Nonius Kappa CCD diffractometer mounted on a FR590 generator equipped with a sealed tube using $Mo_{K\alpha}$ ($\lambda = 0.71073$ Å) radiation and a graphite monochromator. The structures were solved using direct methods (SHELXS-97), and were refined by the full-matrix least-squares technique on F^2 with SHELXL-97.[43]

Complex 1: $C_6H_{18}ClO_3RhS_3$, orange, elongated parallelogram, $0.4 \times 0.1 \times 0.1$ mm, monoclinic, $P2_1/c$ (No. 14), $a = 5.7250(11)$, $b = 15.932(3)$, $c = 14.368(3)$ Å, $\beta = 90.58(3)°$, $V = 1310.4(5)$ Å^3, $Z = 4$, $Fw = 372.74$, $\rho_{calcd} = 1.889$ mg m^{-3}, $\mu = 1.966$ mm^{-1}. The final cycle of refinement based on F^2 gave an agreement factor of $R = 0.028$ for data with $I > 2\sigma(I)$ and $R = 0.031$ for all data (2076 reflections), with a goodness-of-fit of 1.006. Idealized hydrogen atoms were placed and refined in riding mode.

Complex 2: $C_6H_{18}ClIrO_3S_3$, green, parallelogram, $0.3 \times 0.3 \times 0.1$ mm, monoclinic, $P2_1/c$ (No. 14), $a = 5.7410(11)$, $b = 15.920(3)$, $c = 14.340(3)$ Å, $\beta = 90.84(3)°$, $V = 1310.5(5)$ Å^3, $Z = 4$, $Fw = 462.03$, $\rho_{calcd} = 2.342$ mg m^{-3}, $\mu = 10.851$ mm^{-1}. The final cycle of refinement based on F^2 gave an agreement factor of $R = 0.031$ for data with $I > 2\sigma(I)$ and $R = 0.044$ for all data (4967 reflections), with a goodness-of-fit of 1.026. Idealized hydrogen atoms were placed and refined in riding mode.

Complex 4: $C_{14}H_{32}Cl_2O_3S_3Rh_2 \cdot$ ½C7. [One organometallic molecule and one solvent molecule (toluene) with half occupancy was found in the asymmetric unit (discreet disorder). The geometric center of the six-carbon atom ring of the toluene molecule was 0.42 Å from the center of inversion (solvent molecule breaks the $P\bar{1}$ symmetry.] Yellow, needles, $0.20 \times 0.05 \times 0.05$ mm, triclinic, $P\bar{1}$ (No. 2), $a = 6.1740(12)$, $b = 12.026(2)$, $c = 17.111(3)$ Å, $\alpha = 88.14(3)$, $\beta = 87.25(2)$, $\gamma = 82.67(3)°$, $V = 1258.2(4)$ Å^3, $Z = 2$, $Fw = 663.36$, $\rho_{calcd} = 1.751$ mg m^{-3}, $\mu = 1.788$ mm^{-1}. The final cycle of refinement based on F^2 gave an agreement factor of $R = 0.034$ for data with $I > 2\sigma(I)$ and $R = 0.049$ for all data (6132 reflections), with a goodness-of-fit of 1.018. Idealized hydrogen atoms were placed and refined in riding mode. No hydrogen atoms were placed on the disordered solvent molecule (toluene).

Complex 5: $C_{20}H_{28}Cl_2O_2S_2Ir_2$ (two molecules are present in the asymmetric unit), yellow, parallelogram, $0.10 \times 0.10 \times 0.05$ mm, triclinic, $P\bar{1}$ (No. 2), $a = 9.4440(19)$, $b = 11.087(2)$, $c = 11.950(2)$ Å, $\alpha = 90.45(3)$, $\beta = 104.32(3)$, $\gamma = 90.93(3)°$, $V = 1212.1(4)$ Å^3, $Z = 2$, $Fw = 819.84$, $\rho_{calcd} = 2.246$ mg m^{-3}, $\mu = 11.374$ mm^{-1}. The final cycle of refinement based on F^2 gave an agreement factor of $R = 0.049$ for data with $I > 2\sigma(I)$ and $R = 0.052$ for all data (4223 reflections), with a goodness-of-fit of 1.020. Idealized hydrogen atoms were placed and refined in riding mode.

Complex 11: $C_{24}H_{48}B_2F_8O_4S_4Rh_2$ (two molecules are present in the asymmetric unit), yellow, parallelogram, $0.5 \times 0.1 \times 0.1$ mm, orthorhombic, $Pca2_1$ (No. 29), $a = 12.317(3)$, $b = 24.171(5)$, $c = 11.808(2)$ Å, $\alpha = 90$, $\beta = 90$, $\gamma = 90°$, $V = 3515.4(12)$ Å^3, $Z = 4$, $Fw = 908.30$, $\rho_{calcd} = 1.716$ mg m^{-3}, $\mu = 1.248$ mm^{-1}. The final cycle of refinement based on F^2 gave an agreement factor of $R = 0.032$ for data with $I > 2\sigma(I)$ and $R = 0.037$ for all data (4561 reflections), with a goodness-of-fit of 1.035. Idealized hydrogen atoms were placed and refined in riding mode.

Complex 12: $C_8H_{24}F_6O_4PRhS_4$, yellow, triangular plate, $0.1 \times 0.1 \times 0.02$ mm, monoclinic, Pc (No. 7), $a = 8.8580(18)$, $b = 5.9930(12)$, $c = 19.061(4)$ Å, $\beta = 92.50(3)°$, $V = 1010.9(4)$ Å^3, $Z = 2$, $Fw = 560.39$, $\rho_{calcd} = 1.841$ mg m^{-3}, $\mu = 1.400$ mm^{-1}. The final cycle of refinement based on F^2 gave an agreement factor of $R = 0.026$ for data with $I > 2\sigma(I)$ and $R = 0.028$ for all data (3089 reflections), with a goodness-of-fit of 1.030. Idealized hydrogen atoms were placed and refined in riding mode.

Complex 14: $C_{14}H_{22}F_6IrN_2O_2PS_2$, pale yellow, rectangular plate, $0.5 \times 0.15 \times 0.05$ mm, monoclinic, $P2_1/n$ (No. 14), $a = 10.616(2)$, $b = 19.234(4)$, $c = 10.619(2)$ Å, $\beta = 92.60(3)°$, $V = 2164.0(7)$ Å^3, $Z = 4$, $Fw = 651.63$, $\rho_{calcd} = 2.000$ mg m^{-3}, $\mu = 6.499$ mm^{-1}. The final cycle of refinement based on F^2 gave an agreement factor of $R = 0.036$ for data with $I > 2\sigma(I)$ and $R = 0.045$

for all data (4613 reflections), with a goodness-of-fit of 1.002. Idealized hydrogen atoms were placed and refined in riding mode.

Complex 17: $C_{12}H_{36}Cl_3Ir_3O_8S_6 \cdot \frac{1}{2}(C_3H_6O)$, yellow, needles, $0.05 \times 0.02 \times 0.02$ mm, monoclinic, $C2/c$ (No. 7), $a = 39.407(9)$, $b = 9.070(2)$, $c = 19.004(4)$ Å, $\beta = 104.13(3)^\circ$, $V = 6587(2)$ Å^3, $Z = 8$, $Fw = 1212.88$, $\rho_{calcd} = 2.446$ mg m^{-3}, $\mu = 12.75$ mm^{-1}. The final cycle of refinement based on F^2 gave an agreement factor of $R = 0.073$ for data with $I > 2\sigma(I)$ and $R = 0.080$ for all data (3427 reflections), with a goodness-of-fit of 1.317. Idealized hydrogen atoms were placed and refined in riding mode.

Complex 18: $C_6H_{20}F_6IrO_4PS_3 + C_2H_6SO$, pale yellow, parallelogram, $0.2 \times 0.1 \times 0.05$ mm, triclinic, $P\bar{1}$ (No. 2), $a = 8.995(2)$, $b = 10.909(2)$, $c = 11.441(2)$ Å, $\alpha = 94.02(3)$, $\beta = 109.76(3)$, $\gamma = 90.49(3)^\circ$, $V = 1053.3(4)$ Å^3, $Z = 2$, $Fw = 667.70$, $\rho_{calcd} = 2.105$ mg m^{-3}, $\mu = 6.877$ mm^{-1}. The final cycle of refinement based on F^2 gave an agreement factor of $R = 0.034$ for data with $I > 2\sigma(I)$ and $R = 0.040$ for all data (5198 reflections), with a goodness-of-fit of 1.006. Idealized hydrogen atoms were placed and refined in riding mode.

Complex 19: $C_{11}H_{33}F_6IrO_7PS_4$, yellow, thin plate, $0.1 \times 0.1 \times 0.02$ mm, orthorhombic, $Pca2_1$, $a = 16.969(3)$, $b = 12.865(3)$, $c = 11.602(2)$ Å, $V = 2532.8(9)$ Å^3, $Z = 4$, $Fw = 934.98$, $\rho_{calcd} = 2.452$ mg m^{-3}, $\mu = 10.964$ mm^{-1}. The final cycle of refinement based on F^2 gave an agreement factor of $R = 0.044$ for data with $I > 2\sigma(I)$ and $R = 0.053$ for all data (2986 reflections), with a goodness-of-fit of 1.024. Idealized hydrogen atoms were placed and refined in riding mode.

CCDC-177298 (complex **1**), CCDC-208420 (complex **2**), CCDC-177299 (complex **4**), CCDC-208318 (complex **5**), CCDC-177300 (complex **11**), CCDC-177301 (complex **12**), CCDC-208316 (complex **14**), CCDC-209609 (complex **17**), CCDC-208522 (complex **18**), and CCDC-208317 (complex **19**) contain the supplementary crystallographic data for this paper. These data can be obtained free of charge via www.ccdc.cam.ac.uk/conts/retrieving.html (or from the Cambridge Crystallographic Data Centre, 12 Union Road, Cambridge CB2 1EZ, UK: fax: (+44) 1223-336-033; or e-mail: deposit@ccdc.cam.ac.uk).

Acknowledgements

This work was supported by the Israel Science Foundation (Jerusalem, Israel), by the MINERVA foundation (Munich, Germany), and by the Levine Fund. D.M. is the holder of the Israel Matz Professorial Chair of Organic Chemistry.

[1] a) R. S. Dickson in *Organometallic Chemistry of Rhodium and Iridium* (Eds.: P. M. Maitlis, F. G. A. Stone, R. West), Academic Press, London, **1983**; b) J. P. Collman, L. S. Hegedus, J. R. Norton, R. G. Finke, *Principles and Applications of Organotransition Metal Chemistry*, University Science, Mill Valley, **1987**.

[2] M. Calligaris, O. Carugo, *Coord. Chem. Rev.* **1996**, *153*, 83.

[3] A Rh^I–DMSO dimer $[RhCl(DMSO)_2]_2$ was characterized based only on its IR spectrum, see: a) B. R. James, R. H. Morris, *Can. J. Chem.* **1980**, *58*, 399. The existence of Ir^I–DMSO complexes was suggested, see: b) B. R. James, R. H. Morris, P. Kvintovics, *Can. J. Chem.* **1986**, *64*, 897.

[4] a) Y. M. Y. Haddad, H. B. Henbest, J. Trocha-Grimshaw, *J. Chem. Soc. Perkin Trans. 1* **1974**, 592, and references therein; b) Y. M. Y. Haddad, H. B. Henbest, J. Husbands, T. R. B. Mitchell, J. Trocha-Grimshaw, *J. Chem. Soc. Perkin Trans. 1* **1974**, 596, and references therein; c) H. B. Henbest, J. Trocha-Grimshaw, *J. Chem. Soc. Perkin Trans. 1* **1974**, 607, and references therein; d) B. R. James, R. H. Morris, *J. Chem. Soc. Chem. Commun.* **1978**, 929, and references therein.

[5] G. W. Parshall, S. D. Ittel, *Homogeneous Catalysis*, 2nd ed., Wiley, New York, **1992**.

[6] a) D. J. Cole-Hamilton, G. Wilkinson, *Nouv. J. Chim.* **1977**, *1*, 141; b) T. Yoshida, T. Matsuda, T. Okano, S. Otsuka, *J. Am. Chem. Soc.* **1979**, *101*, 2027; c) J. Gotzig, R. Werner, H. Werner, *J. Organomet. Chem.* **1985**, *290*, 99; d) R. S. Paonessa, A. L. Prignano, W. C. Trogler, *Organometallics* **1985**, *4*, 647; e) D. Milstein, J. C. Calabrese, I. D. Williams, *J. Am. Chem. Soc.* **1986**, *108*, 6387; f) M. B. Sponsler, B. H. Weiller, P. O. Stoutland, R. G. Bergman, *J. Am. Chem. Soc.* **1989**, *111*, 6841; g) R. C. Stevens, R. Bau, D. Milstein, O. Blum, T. Koetzle, *J. Chem. Soc. Dalton Trans.* **1990**, 1429; h) H. Werner, A. Michenfelder, M. Schulz, *Angew. Chem.* **1991**, *103*, 555; *Angew. Chem. Int. Ed. Engl.* **1991**, *30*, 596; i) F. T. Ladipo, M. Kooti, J. S. Merola, *Inorg. Chem.* **1993**, *32*, 1681; j) M. J. Burn, M. G. Fickes, J. F. Hartwig, F. J. Hollander, R. G. Bergman, *J. Am. Chem. Soc.* **1993**, *115*, 5875; k) O. Blum, D. Milstein, *Angew. Chem.* **1995**, *107*, 210; *Angew. Chem. Int. Ed. Engl.* **1995**, *34*, 229; l) R. Dorta, A. Togni, *Organometallics* **1998**, *17*, 3423; m) K. Tani, A. Iseki, T. Yamagata, *Angew. Chem.* **1998**, *110*, 3590; *Angew. Chem. Int. Ed. Engl.* **1998**, *37*, 3381; n) D. Morales-Morales, D. W. Lee, Z. Wang, C. M. Jensen, *Organometallics* **2001**, *20*, 1144; o) O. Blum, D. Milstein, *J. Am. Chem. Soc.* **2002**, *124*, 11456.

[7] a) R. Dorta, H. Rozenberg, L. J. W. Shimon, D. Milstein, *J. Am. Chem. Soc.* **2002**, *124*, 188; b) R. Dorta, H. Rozenberg, D. Milstein, *Chem. Commun.* **2002**, 710.

[8] The reported dimer $[Rh_2Cl_2(DMSO)_4]$ may actually be complex **1**, see reference [3].

[9] A. Cusanelli, U. Frey, A. E. Merbach, *Chem. Commun.* **1997**, 379.

[10] It has been shown for other transition-metal complexes that the *trans* arrangement of S-bound DMSO is not very favorable, see reference [2].

[11] M. J. Bennett, P. B. Donaldson, *Inorg. Chem.* **1977**, *16*, 655.

[12] Quite surprisingly, a data search showed that complexes of the type $[IrCl(PR_3)_3]$ have never been characterized by X-ray crystallography, and thus structural comparison of complex **2** with its phosphine analogues was not possible.

[13] T. Tamase, T. Aiko, Y. Yamamoto, *Chem. Commun.* **1996**, 2341.

[14] S. Geremia, S. Mestroni, M. Calligaris, E. Allesio, *J. Chem. Soc. Dalton Trans.* **1998**, 2447.

[15] F. A. Cotton, E. V. Dikarev, M. A. Petrukhina, S.-E. Stiriba, *Inorg. Chem.* **2000**, *39*, 1748; these two compounds were obtained by synthesis in the absence of solvent, and could only be observed in the solid state.

[16] M. Calligaris, P. Faleschini, E. Alessio, *Acta Crystallogr. Sect. C* **1991**, *47*, 747.

[17] E. Alessio, P. Faleschini, A. Sessanta o Santi, G. Mestroni, M. Calligaris, *Inorg. Chem.* **1993**, *32*, 5756.

[18] For detailed reactivity studies of $[Ir_2Cl_2(cod)_2]$ towards phosphine ligands, see: B. Denise, G. Pannetier, *J. Organomet. Chem.* **1978**, *148*, 155, and references therein.

[19] These compounds are excellent hydrogenation catalysts, for example: W. De Aquino, R. Bonnaire, C. Potvin, *J. Organomet. Chem.* **1978**, *154*, 159, and references cited therein.

[20] D. A. Ortmann, B. Weberndörfer, K. Ilg, M. Laubender, H. Werner, *Organometallics* **2002**, *21*, 2369.

[21] For reactivity studies of complexes **9** and **13**, see: R. Dorta, L. J. W. Shimon, H. Rozenberg, D. Milstein, *Eur. J. Inorg. Chem.* **2002**, 1827.

[22] Complex **10** reacts with benzyl chloride in much the same way as complex **9**; R. Dorta, D. Milstein, unpublished results.

[23] M. Green T. A. Kuc, *J. Chem. Soc. Dalton Trans.* **1972**, 832.

[24] B. R. James, R. H. Morris, K. J. Reimer, *Can. J. Chem.* **1977**, *55*, 2353.

[25] For details see the data deposited at the CCDC.

[26] In this context, it is interesting to note that sulfoxides can be forced to bind through their sulfur atoms to such cationic Rh^I–COD complexes. Chelating ethylene-bridged bis(sulfoxides) of this kind have been characterized based on spectroscopic data, see: a) C. Pettinari, M. Pellei, G. Cavicchio, M. Crucianelli, W. Panzeri, M. Colapietro, A. Cassetta, *Organometallics* **1999**, *18*, 555; b) D. R. Evans, M. Huang, W. M. Seganish, J. C. Fettinger, T. L. Williams, *Inorg. Chem. Commun.* **2003**, *6*, 462.

[27] For the preparation of $[Rh(coe)_2(O{=}CMe_2)_2]PF_6$, see: a) B. Windmuller, O. Nürnberg, J. Wolf, H. Werner, *Eur. J. Inorg. Chem.* **1999**, 613; for its X-ray structure, see: b) H. Werner, M. E. Schneider, M. Bosch, J. Wolf, J. H. Teuben, A. Meetsma, S. I. Troyanov, *Chem. Eur. J.* **2000**, *6*, 3052.

[28] For the isolation, characterization, as well as the reactivity of this complex towards alkylphosphines, see: R. Dorta, R. Goikhman, D. Milstein, *Organometallics* **2003**, *22*, 2806.

[29] H. M. Lee, T. Jiang, E. D. Stevens, S. P. Nolan, *Organometallics* **2001**, *20*, 1255.

[30] M. S. Abbassioun, P. B. Hitchcock, P. A. Chaloner, *Acta Crystallogr. Sect. C* **1989**, *45*, 953.

[31] Ir *trans*-dihydride complexes give rise to ^{1}H NMR signals at a significantly lower field than *cis*-dihydride ones, see for example: a) S.

Nemeh, R. J. Flesher, K. Gierling, C. Maichle-Mossmer, H. A. Mayer, W. C. Kaska, *Organometallics* **1998**, *17*, 2003; b) B. Rybtchinksi, Y. Ben-David, D. Milstein, *Organometallics* **1997**, *16*, 3786.

[32] Analysis of the rate is approximate as the DMSO molecules of the starting complex exchange rapidly with the deuterated solvent. Thus, completion of the reaction was observed by comparing the integration of the hydride peak with the signal for one of the free, non-deuterated DMSO molecules.

[33] For a review, see: B. R. James in *Comprehensive Organometallic Chemistry* (Eds.: G. Wilkinson, F. G. A. Stone, E. W. Abel), Pergamon, New York, **1982**.

[34] C. E. Johnson, R. Eisenberg, *J. Am. Chem. Soc.* **1985**, *107*, 3148.

[35] It has been shown that oxidative addition of OH bonds to neutral, electron-rich iridium phosphine complexes occurs by nucleophilic attack of 16-electron species of the type $[IrCl(PR_3)_3]$ (R = methyl, ethyl) on the OH proton (see reference [6o]). The fact that the 16-electron complexes **7** and **8** do not undergo water oxidative addition is probably a result of their not being nucleophilic enough on the one hand, and capable of forming a reactive 14-electron species on the other.

[36] A. L. Casalnuovo, J. C. Calabrese, D. Milstein, *J. Am. Chem. Soc.* **1988**, *110*, 6738.

[37] The NMR spectrum of a mixture of these two compounds did not give clear results because of the low solubility of these complexes and, possibly, because exchange processes rendered analysis difficult (see also the discussion of complexes **17** and **18**).

[38] Protonation of the PF_6^- counterion was also observed during the reaction of complex $[Ir(coe)_2(O{=}CMe_2)_2]PF_6$ with water: R. Dorta, D. Milstein, unpublished results.

[39] P. Hofmann, C. Meier, U. Englert, U. Schmidt, *Chem. Ber.* **1992**, *125*, 353.

[40] R. H. Crabtree, S. M. Morehouse, J. M. Quirk, *Inorg. Synth.* **1986**, *24*, 173.

[41] M. Green, T. A. Kuc, S. H. Taylor, *J. Chem. Soc. A* **1971**, 2334.

[42] A. Van der Ent, A. L. Onderlinden, *Inorg. Synth.* **1990**, *28*, 90.

[43] G. M. Sheldrick, SHELX-97, Program for Crystal Structure Refinement, University of Göttingen, Göttingen (Germany), **1997**.

Received: May 15, 2003 [F5144]

